

Published in: *Journal of Neurophysiology* **122**: 1473-1490 (2019).

Metabolic constraints on synaptic learning and memory

Jan Karbowski^{a,b}

^(a) *Institute of Applied Mathematics and Mechanics,*

University of Warsaw, ul. Banacha 2, 02-097 Warsaw, Poland;

^(b) *Nalecz Institute of Biocybernetics and Biomedical Engineering,*

Polish Academy of Sciences, 02-109 Warsaw, Poland

Abstract

Dendritic spines, the carriers of long-term memory, occupy a small fraction of cortical space, and yet they are the major consumers of brain metabolic energy. What fraction of this energy goes for synaptic plasticity, correlated with learning and memory? It is estimated here based on neurophysiological and proteomic data for rat brain that, depending on the level of protein phosphorylation, the energy cost of synaptic plasticity constitutes a small fraction of the energy used for fast excitatory synaptic transmission, typically 4.0 – 11.2%. Next, this study analyzes a metabolic cost of a new learning and its memory trace in relation to the cost of prior memories, using a class of cascade models of synaptic plasticity. It is argued that these models must contain bidirectional cyclic motifs, related to protein phosphorylation, to be compatible with basic thermodynamic principles. For most investigated parameters longer memories generally require proportionally more energy to store. The exception are the parameters controlling the speed of molecular transitions (e.g. ATP driven phosphorylation rate), for which memory lifetime per invested energy can increase progressively for longer memories. Furthermore, in general, a memory trace decouples dynamically from a corresponding synaptic metabolic rate such that the energy expended on a new learning and its memory trace constitutes in most cases only a small fraction of the baseline energy associated with prior memories. Taken together, these empirical and theoretical results suggest a metabolic efficiency of synaptically stored information.

Email: jkarbowski@mimuw.edu.pl

Keywords: energy cost of learning and memory; molecular mechanisms of synaptic plasticity; ATP-driven reactions; phosphorylation; cascade models; memory lifetime; metabolism; non-equilibrium steady state; entropy production.

Author Summary:

Learning and memory involve a sequence of molecular events in dendritic spines, called synaptic plasticity. These events are physical in nature and require energy, which has to be supplied by ATP molecules. However, our knowledge of the energetics of these processes is very poor. This study estimates the empirical energy cost of synaptic plasticity, and considers theoretically a metabolic rate of learning and its memory trace in a class of cascade models of synaptic plasticity.

INTRODUCTION

Brain is one of the most expensive organs in the body (Aiello and Wheeler 1995; Attwell and Laughlin 2001; Clarke and Sokoloff 1994), and larger brains consume correspondingly more energy (Karbowski 2007, 2011). Data indicate that much of this energy is used by synapses (Harris et al 2012; Karbowski 2014). For example, it was estimated that fast excitatory synaptic transmission requires $1.4 \cdot 10^5$ ATP molecules per presynaptic stimulation to pump out an influx of Na^+ ions (Attwell and Laughlin 2001), which assuming 1 Hz for such stimulation in the rat cortex (see below) yields a metabolic rate of $8.4 \cdot 10^6$ ATP/min per spine.

High metabolic requirement of synapses is also visible during mammalian brain development when cerebral metabolic rate changes in proportion to changes in synaptic density (Karbowski 2012). On the other hand, imaging experiments show that brain stimulation increases cerebral metabolic rate only weakly by $\sim 10\%$ from its resting (baseline) value (Shulman and Rothman 1998; Shulman et al 1999), which may suggest that housekeeping processes in the brain are more energy demanding than acquiring and processing of a new information (Shulman et al 2004; Raichle and Mintun 2006). Interestingly, recent data on cortical stimulation and energetics of synaptic transmission in rodents reveal that the small increase in the cortical metabolic rate is shared proportionally between neurons and astrocytes (Sonnay et al 2016, 2018), implying that both neuronal and glial compartments are important for synaptic function.

Learning and memory in the brain is strictly associated with plasticity mechanisms in synapses (Lisman et al 2012; Kandel et al 2014; Takeuchi et al 2014; Poo et al 2016). There exist a huge literature on modeling of synaptic plasticity and memory (for reviews

see e.g. Bhalla 2014; Chaudhuri and Fiete 2016), but virtually all of it neglects the energetic aspect. This omission is surprising, because most of what we know about real time brain workings is based on imaging techniques, which rely on brain metabolism (Shulman et al 2004; Raichle and Mintun 2006). Moreover, molecular processes in synapses are physical in nature and require a permanent energy influx to counteract dissipation, which is related to ATP (and/or GTP) hydrolysis (Engl and Attwell 2015; Rolfe and Brown 1997; Phillips et al 2012). This means that there should exist some cost to learning and memory in the brain, and an open fundamental question is how big is it, and to what extent it can constrain the strength and duration of a memory trace?

Synaptic plasticity mechanisms related to long term potentiation (LTP) and depression (LTD) are induced by calcium influx to a dendritic spine through NMDA and voltage-gated receptors, and subsequent activation of various enzymes, such as CAMKII, PSD-95, protein kinase A and C, MAPK, etc (Lisman et al 2012; Kandel et al 2014; Bhalla and Iyengar 1999). These enzymes serve as upstream initiators of complex molecular signaling pathways from spine membrane to postsynaptic density (PSD), within PSD, and beyond in the form of protein activation cascades (Sheng and Hoogenraad 2007; Zhu et al 2016). The most common mechanism of protein activation is by phosphorylation (adding of a phosphate group), which is powered by ATP hydrolysis (Qian 2007), and it was found that many PSD proteins are phosphorylated during initiation of LTP and LTD (Coba et al 2009; Li et al 2016). Thus, protein phosphorylation cascades provide a basic biochemical mechanism of signal transduction in plastic synapses. The end product of the phosphorylation cascades is protein synthe-

sis in PSD, actin polymerization, and AMPA receptor trafficking on spine membrane (Cingolani and Goda 2008; Lisman et al 2012; Bosch et al 2014). All of these processes influence synaptic conductance/weight (Kasai et al 2003; Meyer et al 2014), and they cause some energy drain (consumption of ATP), which magnitude is essentially unknown. This paper provides an estimate of the metabolic cost of these reactions.

Phenomenological models of cascade synaptic plasticity mimic the richness of biochemical pathways in dendritic spines and provide simple means to study theoretically synaptic memory maintenance (Fusi et al 2005; Leibold and Kempter 2008; Barrett et al 2009; Benna and Fusi 2016). Recent developments within these models shed light on the importance of internal synaptic complexity, i.e. bidirectionality of synaptic transitions and multiple time scales, for producing long memory lifetimes (Benna and Fusi 2016). The aim of this study is to consider the energy requirement for learning and maintaining of a new information in relation to the baseline cost of synaptic plasticity in a class of cascade models. It is argued that these models, in order to be a minimally physically realistic, must contain bidirectional transitions and cyclic motifs (modeled here as phosphorylation-dephosphorylation biochemical reactions). These two features are necessary to generate nonzero and finite synaptic metabolic rate at a steady state, corresponding to a baseline synaptic activity, which presumably stores the memories of all previous plasticity events. Keeping these memories is physically associated with maintaining synaptic structure and processes, and this requires an energy influx to counteract dissipation. This implies that synapses in the steady state or during baseline activity must operate out of thermal equilibrium to freely exchange energy and material with their environment (neurons, glia). This is similar to the behavior of all

biological systems that have to be in nonequilibrium state to avoid “thermal death” (Hill 1989; Nicolis and Prigogine 1977; Qian 2006).

RESULTS

Estimates of energy requirements of various molecular processes involved in synaptic plasticity.

Synaptic plasticity of excitatory synapses, i.e. change in synaptic conductance (weight) and size, involves a sequence of molecular events and can be broadly divided into three categories: extra-synaptic (outside dendritic spine), intra-synaptic (inside the spine), and modulatory. Below we estimate ATP rates associated with each of these contributions to the plasticity based on empirical data for rat brain.

Extra-synaptic cost.

Extra-synaptic input is necessary for the initiation of synaptic plasticity. In particular, the induction of synaptic plasticity requires the influx of Ca^{+2} ions to the dendritic spine (Miller et al 2005; Lisman et al 2012). Calcium signal serves as a trigger of various downstream molecular pathways necessary to induce LTP and/or LTD, with the end result of changing the spine conductance weight and size (Lisman et al 2012; Poo et al 2016). We consider two types of the extra-synaptic costs: plasticity related glutamate recycling via astrocytes (Sonnay et al 2016, 2018), and plasticity related ATP release from astrocytes that binds to the spine membrane (Khan and North 2012), as the energy associated with these two processes is directly linked to the energy cost of synaptic plasticity initiation, i.e. calcium entering the spine.

Plasticity related glutamate recycling.

The number of glutamate molecules released by one vesicle of a presynaptic terminal is large (~ 4000 plus about 1/3 of that number released from a neighboring astrocyte;

see Attwell and Laughlin (2001) and Jourdain et al (2007)). However, for plasticity initiation only a small fraction of this number matters, and these are glutamates that bind directly to NMDA spine receptors to allow Ca^{2+} influx. There are roughly 10 NMDA receptors on the spine (Nimchinsky et al 2004), each binding 1 glutamate, with a stimulation rate equal to the presynaptic firing rate times the neurotransmitter release probability. The average firing rate in rat cortex is about 4-5 Hz (Schoenbaum et al 1999; Fanselow and Nicolelis 1999; Attwell and Laughlin 2001; Karbowski 2009), while the release probability at these frequencies is about 0.25 (Volgushev et al 2004), which yields about 1 Hz for the rate of NMDA stimulation. When glutamate unbinds from NMDA, it is recycled for the next use. Approximately 2.67 ATP molecules have to be hydrolyzed for each recycled glutamate (Attwell and Laughlin 2001), which happens mostly through astrocytes and involves several steps, such as glutamate uptake, its metabolic processing and conversion to glutamine, glutamine transporting to neurons, and glutamate packing into vesicles (Sonnay et al 2016, 2018). Thus in total, the plasticity related glutamate recycling ATP rate is $10 \cdot 2.67 \text{ ATP/s}$ or 1602 ATP/min .

Plasticity related ATP release from astrocytes and binding to spines.

Another molecule that binds to the spine receptors is ATP, which in this case plays the role of a transmitter (Khan and North 2012). ATP released from astrocytes can activate purinergic P2X receptors (by transducing its energy), which are known to modulate synaptic plasticity (Pankratov et al 2009), allowing calcium to enter the spine (see also below the section “plasticity modulation”). It was measured that the postsynaptic current through P2X receptors constitutes only about 10% of the current passing through glutamate receptors, mostly AMPA (Khan and North 2012). Since the

number of AMPA on the spine is about 100 (Matsuzaki et al 2001), this suggests that the number of P2X is about 10 (P2X and AMPA channels have comparable conductances; Khakh and North 2012). Each P2X binds 3 ATP molecules for its activation (Bean et al 1990). The rate of ATP release from astrocytes is not known (it is likely activity dependent), but we can assume that the timing between two consecutive releases should be at least as long as the ATP binding time constant, which for most of P2X receptors is long and more than 20 sec. Assuming 30 sec, this gives us 30 released ATP molecules related to plasticity per 30 sec, or the consumption rate of 60 ATP/min.

Intra-synaptic cost.

Below we estimate the energy requirements for the basic molecular processes inside a dendritic spine, which are related to plasticity induction and maintenance. These include: Ca^{2+} intra-spine trafficking, protein phosphorylation, protein synthesis (turnover), actin treadmilling, and receptor (AMPA and NMDA) trafficking.

Ca^{2+} removal.

Following a presynaptic action potential or postsynaptic backpropagation calcium flows into the spine (either through NMDA channels or voltage sensitive Ca^{2+} channels) and trigger a cascade of molecular processes, initiating the synaptic plasticity. For a spine volume of $0.1 \mu\text{m}^3$ (Honkura et al 2008), it was found that about 2000 Ca^{2+} ions enter, of which about 95% bind to endogenous buffers (Sabatini et al 2002). The remaining 100 Ca^{2+} are free and can activate CaMKII (and possibly other) proteins, but they have to be pumped out after the activation to recover baseline physiological conditions of resting calcium concentration in the spine. The rate of the extrusion is given by presynaptic stimulation (1 Hz), and is conducted by Ca^{2+} -ATP pumps or $\text{Na}^+ \text{-Ca}^{2+}$

exchanger. Since both of these processes hydrolyze 1 ATP molecule per 1 removed Ca^{2+} ion, we find the ATP hydrolysis rate of calcium extrusion from the spine 100 ATP/s or 6000 ATP/min.

Protein phosphorylation.

Protein phosphorylation is the main activation mechanism of downstream proteins, actin, AMPA receptors, and other spine molecules, and thus it is of prime importance (Zhu et al 2016). One cycle of protein phosphorylation requires the hydrolysis of 1 ATP molecule (Hill 1989; Qian 2007). First, we estimate the ATP consumption rate for resting non-LTP related phosphorylation, i.e. for unstimulated spine with resting Ca^{2+} concentration, and then for stimulated spine undergoing LTP.

In general, for the resting spine the levels of protein phosphorylation rates seem to be uniformly distributed and vary by two orders of magnitude, from 0.001 min^{-1} to 0.34 min^{-1} (Molden et al 2014), which yields an average value of 0.15 min^{-1} . There are about 10^4 proteins (including their copies) in the spine PSD (Sheng and Kim 2011), with an average of 4-6 phosphorylation sites per protein (Collins et al 2005; Trinidad et al 2012). This gives the resting rate of ATP-driven protein phosphorylation as $(6 - 9) \cdot 10^3 \text{ ATP/min}$, with an average of 7500 ATP/min. Because hydrolysis of one ATP requires 20 kT , where k is the Boltzmann constant and T is the absolute temperature (Phillips et al 2012), we obtain equivalently the resting energy rate of protein phosphorylation as $15 \cdot 10^4 \text{ kT/min}$ in a single spine. This ATP rate is however unrelated to learning and memory, since the resting conditions (unstimulated spine) do not drive plasticity events, i.e., changes in AMPA receptor number.

More relevant rates for LTP-related ATP consumption can be obtained by noting

that during the plasticity induction, stimulated by Ca^{2+} influx to the spine, the phosphorylation rates of about 10% PSD proteins are strongly enhanced as the proteins interact more frequently (about 130 proteins out of roughly 1500; Coba et al 2009; Li et al 2016; Bayes et al 2012). The important point is that this fraction is dependent on the frequency of Ca^{2+} stimulation (De Koninck and Schulman 1998; Gaertner et al 2004). For example, the rate of CaMKII autophosphorylation jumps 3 – 4 orders of magnitude, from the resting of 0.03 min^{-1} (Colbran 1993; Miller et al 2005) to about $60 - 600 \text{ min}^{-1}$ (Bradshaw et al 2002; Miller et al 2005; Michalski 2013), but this amplified phosphorylation takes place only for a few percent of CaMKII at about 1 Hz of Ca^{2+} influx (De Koninck and Schulman 1998; Gaertner et al 2004). We can expect that during continuing calcium stimulation, as for regular *in vivo* cortical conditions, some balance between proteins highly phosphorylated and those at resting phosphorylation is achieved. In such a stationary state, both of these protein groups contribute to the ATP consumption rate, which can be written as:

$$A\dot{T}P_{phos} = N[(1 - x)r_r M_s + xr_a M_s^*],$$

where $N(= 10^4)$ is the total number of proteins (including their copies) in PSD, $x(= 0.1)$ is the fraction of proteins with amplified phosphorylation, $M_s(= 5)$ is the average number of phosphorylation sites per protein, M_s^* is the average number of such sites per protein that become highly phosphorylated upon stimulation (M_s^* can be any integer between 1 and 5). M_s^* depends on the frequency of Ca^{2+} stimulation, and it likely assumes its lowest values $\approx 1 - 2$ (De Koninck and Schulman 1998; Gaertner et al 2004). Finally, r_a and r_r denote the average rates for active and resting phosphorylation (population averaged resting $r_r = 0.15 \text{ min}^{-1}$). There are virtually no data on r_a in

PSD proteins other than CaMKII. For this reason, in our estimate we take for r_a a medium value of the numbers reported for CaMKII, i.e., $r_a \approx 300 \text{ min}^{-1}$. Using the above parameters, we obtain the steady-state ATP consumption rate during LTP phase as $\dot{ATP}_{phos} = 3.1 \cdot 10^5 \text{ ATP/min}$ for $M_s^* = 1$, and $\dot{ATP}_{phos} = 9.1 \cdot 10^5 \text{ ATP/min}$ for $M_s^* = 3$. These values correspond respectively to 20% and 60% of the protein sites with enhanced phosphorylation.

As a curiosity, let us estimate the above \dot{ATP}_{phos} for different values of the fraction of highly activated proteins x . First, note that for $x = 0$ (no proteins with amplified phosphorylation), the \dot{ATP}_{phos} is exactly equal to the resting non-LTP phosphorylation cost calculated above. Next, since \dot{ATP}_{phos} increases with x , we want to find out for what value of x the ATP cost of protein phosphorylation is equal to the cost of fast synaptic transmission ($8.4 \cdot 10^6 \text{ ATP/min}$)? For $M_s^* = 1$ this never happens, and the maximal value of \dot{ATP}_{phos} in this case is $3 \cdot 10^6 \text{ ATP/min}$, which is 36% of the fast synaptic transmission cost. For $M_s^* = 3$ this happens when $x = 0.94$, i.e., almost all PSD proteins would have to be activated by phosphorylation. For the maximal value of $M_s^* = 5$, this situation occurs for $x = 0.56$, i.e. half of the proteins must be highly activated. Finally, the maximal possible value of \dot{ATP}_{phos} is $15 \cdot 10^6 \text{ ATP/min}$ (all PSD proteins are maximally phosphorylated), which is nearly twice the cost of fast synaptic transmission. The latter hypothetical calculation is useful, because it sets the upper bound on the possible error in estimating the overall cost of synaptic plasticity.

It is interesting to estimate what fraction of the resting global phosphorylation cost is taken by two the most abundant proteins: CaMKII (α and β subunits) and PSD-95. There are 5600 copies of CaMKII α and CaMKII β in a spine (Sheng and Kim 2011), and

both subunits have similar number of 10 phosphorylation sites (Trinidad et al 2006). The number of copies of the PSD-95 protein in a spine is 300 (Sheng and Kim 2011), and it has between 8 and 12 phosphorylation sites (Trinidad et al 2006; Zhang et al 2011). Assuming that both proteins have the same resting phosphorylation rates, i.e., 0.03 min^{-1} , corresponding to CaMKII autophosphorylation, we get the energy rate 1700 ATP/min for CaMKII, and $60 - 100 \text{ ATP/min}$ for PSD-95. If we combine these two numbers, we get that these two proteins consume $20 - 30\%$ of the global resting phosphorylation energy rate of the whole postsynaptic density PSD. This indicates that these two plentiful proteins, comprising about 60% of the PSD content, consume a substantial part of the whole energy devoted to protein phosphorylation during resting non-LTP spine conditions.

Protein synthesis/turnover.

The cost of protein turnover is estimated as follows. The total molecular mass of a typical PSD has been calculated as $1.1 \cdot 10^9 \text{ Da}$ (Chen et al 2005), and this corresponds to a total number of 10^7 amino acids, which are bound by the same number of peptide bonds that require 4 ATP molecules/bond to form (Engl and Attwell 2015). The average half-lifetime of PSD proteins is 3.67 days (Cohen et al 2013), which means that after that time a half of all peptide bonds are broken. This means that the ATP consumption rate for protein synthesis as $3.7 \cdot 10^3 \text{ ATP/min}$ (or equivalently $7.4 \cdot 10^4 \text{ kT/min}$) for a single spine.

Similarly, we also estimate the fraction of global protein synthesis cost taken by CaMKII and PSD-95. Two subunits CaMKII α and CaMKII β have similar molecular masses with an average length of 528 amino acids, while PSD-95 has 779 amino acids

(Yoshimura et al 2004). The half-times for CAMKII decay is 3.4 days (average of 3.0 for CaMKII α and 3.8 for CaMKII α) and for PSD-95 decay is 3.67 days (Cohen et al 2013). Given that there are 5600 copies of CaMKII and 300 copies of PSD-95 (Sheng and Kim 2011), this yields a synthesis rate 0.57 copies/min of CaMKII, and 0.03 copies/min of PSD-95. This requires $4 \cdot 528 \cdot 0.57 = 1200$ ATP/min for CaMKII and $4 \cdot 779 \cdot 0.03 = 93$ ATP/min for PSD-95. From this, it follows that these two the most frequent proteins consume for their synthesis about 1/3 of the total energy used for protein synthesis in the whole PSD.

Actin treadmilling.

Actin treadmilling energetics in spines can be estimated as follows. Each cycle of actin treadmilling involves 1 ATP. Actin concentration in the mammalian brain is $100 \mu\text{M}$ (Devineni et al 1999), which yields 6000 actin molecules per spine (average spine volume assumed: $0.1 \mu\text{m}^3$ (Honkura et al 2008)). About 90 % of actin in spines degrades fast with a characteristic lifetime ~ 40 sec, and the remaining 10 % with much longer time ~ 17 min (Honkura et al 2008; Star et al 2002), which can be neglected. This means that the metabolic cost of actin turnover is 8100 ATP/min (or $1.6 \cdot 10^5 \text{ kT/min}$).

AMPA and NMDA trafficking.

The energy cost of AMPA and NMDA receptor trafficking within a spine is composed of receptor insertion/removal to/from the spine membrane (Huganir and Nicoll 2013) and receptor movement along the membrane (Choquet and Triller 2013). First, we consider the receptor insertion (exocytosis) and removal (endocytosis) contributions. Both of these processes can be envisioned as molecular crossing of energy barriers, because both of them lead to deformations in the membrane structure. The interesting

point is that the rates of endo- and exocytosis of AMPA receptors are very similar at steady state and about 0.1 min^{-1} (Ehlers 2000, Lin et al 2000), which is much faster than the turnover (degradation) rates for AMPA (half-life about 2 days; Cohen et al 2013). The approximate equality of the insertion and removal rates indicates that the energy barriers for these two opposing processes are similar (invoking the Arrhenius law). A typical energy barrier for AMPA insertion is $4 - 30 \text{ kT}$, with an average of 17 kT , which is the energy of protein insertion into a lipid membrane by a mechanism of membrane fusion (Grafmuller et al 2009; Gumbart et al 2011; Francois-Martin et al 2017). Since an average spine contains about 100 AMPA (Matsuzaki et al 2001), we obtain the energy rate for AMPA endocytosis/exocytosis as $2 \cdot 100(17kT) \cdot 0.1 \text{ min}^{-1}$ (the prefactor 2 comes from including both endo- and exocytosis transitions), which yields 340 kT/min , or equivalently 17 ATP/min . Inclusion of NMDA receptors affects this figure by only 10%, since the number of NMDA receptors on spine membrane is much lower, about 10 (Nimchinsky et al 2004). Thus, the total cost of AMPA and NMDA insertion/internalization is 18.7 ATP/min .

Energy requirement of receptor movement is estimated assuming that most of it is done along spine membrane, which might be an underestimate given that some trafficking might also take place internally along actin filaments (Choquet and Triller 2013). In general, the motion of molecules along some substrate is powered by ATP hydrolysis (Bustamante et al 2005), with a generation of a propulsion force F of the order of 6 pN (Visscher et al 1999). Additionally, it was found that AMPA motion along spine membrane was alternating between the periods of diffusion and quietness (Borgdorff and Choquet 2002) with comparable durations, and a diffusion coefficient $D = 0.02 - 0.05$

$\mu\text{m}^2/\text{s}$, or its average value $D = 0.035 \mu\text{m}^2/\text{s}$. The power P dissipated by one receptor is proportional to the product of the force F and an average velocity v , which is $v \sim L/\tau$, where L is the average spine length and τ is the typical time to travel distance L . Since for diffusive processes $\tau \sim L^2/D$ (Phillips et al 2012), we get that velocity $v \sim D/L$. Thus, we can write that the power dissipated by a single receptor trafficking along spine membrane is $P \approx 0.5FD/L$, where the prefactor 0.5 comes from the assumption that the time intervals of diffusion and quietness are roughly similar (Borgdorff and Choquet 2002), which reduces the effective velocity by half. For a typical spine length of $L = 1\mu\text{m}$, we obtain $P \approx 1.05 \cdot 10^{-19} \text{ J/s}$, which using the fact that kT is $4.23 \cdot 10^{-21} \text{ J}$ at 36°C , yields $P \approx 24.8 \text{ kT/s}$, or 74.4 ATP/min . Given that there are 100 AMPA and 10 NMDA receptors in a typical spine (Matsuzaki et al 2001; Nimchinsky et al 2004), we find the energy rate related to receptor movement as 8184 ATP/min (or $1.6 \cdot 10^5 \text{ kT/min}$). This figure is 437 times larger than the one for receptor insertion and internalization, and hence it is much more important.

Plasticity modulation cost.

There are many routes for modulation of synaptic strength. One of the better studied pathways is through purinergic P2X receptors (Pankratov et al 2009; Khakh and North 2012). Activated by ATP molecules P2X receptors, which are voltage gated nonselective channels, enable Ca^{2+} ions to flow inside the spine. This calcium influx modulates various internal molecular pathways, with the end result of affecting the number of AMPA receptors on the spine membrane, likely by modulating their endo- and exocytosis rates (Gordon et al 2005; Pougnat et al 2014). Both LTP and LTD had been observed, depending on which pathway is influenced, but the relative changes

in the synaptic strength did not exceed 30 – 40% (Gordon et al 2005; Pougnet et al 2014). This means that the rates of AMPA insertion and removal should be also affected by this percentage, which suggests that the overall energy rate for AMPA trafficking can increase by about 35% due to the actions of P2X receptors. This translates to an additional 2871 ATP/min. Because of other possible pathways modulating synaptic plasticity, e.g., by adenosinergic receptors, this figure should be considered as a minimal amount of ATP rate due to plasticity modulation.

Summary of the molecular costs.

From these consideration it follows that the intra-synaptic processes are the most energy demanding for the plasticity. Within them, the cost of protein phosphorylation dominates over the rest by a factor 10 – 30. The cost of the remaining intra-synaptic processes (Ca^{2+} removal, actin treadmilling, receptor trafficking) is very similar, with the cost of protein synthesis about two times lower (Table 1). Together, all the synaptic plasticity processes considered here use $(3.4 - 9.4) \cdot 10^5$ ATP/min and account for only about 4 – 11% of the metabolic cost related to the fast excitatory synaptic transmission for rat brain (Table 2). Overall, the small values of these percentages indicate that synaptic plasticity is metabolically inexpensive.

Modeling the metabolic cost of learning and memory.

The next major goal is to study theoretically the energy rate associated with a particular form of learning and memory, and relate it to the lifetime of a new memory.

Motivation for the approach.

All the processes considered above and associated with synaptic plasticity constitute a physical backbone of synaptic learning and memory. We want to quantify the metabolic cost of a new learning and its memory trace, using a modeling approach. To do this, one should in principle include all the above processes in a model. However, combining all of them in a single model is extremely difficult and perhaps even infeasible, because it is not clear how all these plasticity related mechanisms are mutually coupled and with what strength. Instead, we focus in the modeling part on the initial phase of synaptic plasticity, called induction of plasticity (or early LTP), during which synapses start to grow and increase their strength, which is associated with learning of a new input and its subsequent decay. The induction phase is accompanied by enhanced phosphorylation of PSD proteins, including AMPA receptors (while trafficking into the spine membrane), which is evident in Table 1. This indicates that protein phosphorylation is the most energetically demanding and dominating process during the plasticity initiation. For this reason, and because protein phosphorylation is the most commonly studied cellular microcircuit (Krebs 1981; Hill 1989; Qian 2007), it is the main component of the modeling part. We neglect in the model the late phase of plasticity (plasticity maintenance or late LTP) during which most of the protein synthesis takes place, because it uses much less energy (Table 1). We also neglect in the

model the other processes from Table 1, which means that the actual metabolic cost of learning and memory could be slightly greater than theoretically calculated below.

The model used for quantifying the energetics of a memory trace and its duration is based on the so-called cascade models of synaptic plasticity (Fusi et al 2005; Leibold and Kempfer 2008; Barrett et al 2009; Benna and Fusi 2016). In short, these models assume that synaptic molecular machinery can be described in terms of discrete probabilistic states, with transitions between the states depicting molecular transformations. However, the classic cascade models can not describe properly protein phosphorylation due to their simplistic topology, i.e., too simple pattern of molecular transitions. Below, the cascade model of plasticity is extended to include protein interactions via phosphorylation-dephosphorylation mechanism, by adding transition motifs with closed loops (Qian 2007).

The expenditure of energy in the model with phosphorylation-dephosphorylation cycles is quantified using the concept of entropy production rate EPR (Hill 1989; Nicolis and Prigogine 1977). In our case, EPR measures the rate of dissipated energy (metabolic rate) in the spine due to transitions between different molecular states (Rolle and Brown 1997; Qian 2006). When a synapse is in thermodynamic equilibrium with its environment, no energy influx enters the synapse, all internal molecular reactions are balanced (forward and backward reaction rates are equal), and the synapse does not dissipate any energy, implying a vanishing metabolic rate and $EPR = 0$. Such a condition corresponds to a “thermal death” when no biological function can be performed, and thus it cannot represent a baseline or resting synaptic state, during which the synapse keeps track of its prior plasticity events, i.e. keeps their memory. The functional baseline

synaptic state is certainly a driven state that requires energy (and material) exchange with the surrounding, and this implies that the synapse must be an open system in thermodynamic nonequilibrium even during its steady state baseline activity. This steady state or baseline must obviously dissipate energy, as the incoming energy flux breaks the balance in the forward and backward rates of the internal molecular reactions (in our case phosphorylation rates), which leads to nonzero EPR and dissipation, as well as to finite synaptic metabolic rate. We will call this baseline synaptic state, the nonequilibrium steady state (NESS), in analogy to the systems considered in nonequilibrium thermodynamics (Lebowitz and Spohn 1999; Mehta and Schwab 2012). Our theoretical NESS state corresponds to the empirical active steady state phosphorylation phase analyzed above as the intra-synaptic cost of plasticity.

When a synapse is stimulated (by Ca^{2+} influx) and the plasticity event initiated, the molecular reactions/transitions are amplified, which leads to perturbations in the distribution of synaptic states and the emergence of the time dependent memory trace associated with this perturbation. The synaptic perturbation also causes an increase in the rate of energy dissipation (EPR), which declines after some time to its baseline level when the stimulation is turned off. The key relationship that we want to explore, is the one between the total energy expended on memory trace and the memory duration.

Thermodynamically realistic model of cascade synaptic plasticity must contain cyclic reactions.

We consider synaptic plasticity as transitions between multiple discrete synaptic states (Montgomery and Madison 2004) (Fig. 1). These states represent internal degrees of freedom of the molecular processes in a dendritic spine. It is assumed that many

states correspond to one synaptic weight, either weak or strong, denoted as up and down (with the symbols + and – in Fig. 1C), and this reflects neurophysiological data on a single synapse level (Petersen et al 1998; O’Connor et al 2005). The vertical transitions between the states in Fig. 1C correspond to conventional plasticity, while the horizontal transitions are related to the so-called metaplasticity (Abraham and Bear 1996). The latter transitions do not lead to changes in the synaptic weight. It turns out that not every configuration of these transitions produces nonequilibrium steady state (NESS), required for nonzero metabolic rate. For instance, a “ladder” structure of synaptic molecular reactions (Fig. 1A) yields a zero EPR (and metabolic rate) at steady state (see Eq. 15 and below in the Methods), which is not realistic. The basic requirement for NESS and nonzero EPR is the presence of cyclic and bidirectional molecular reactions, which generate nonzero probability flux that mimics the exchange of energy with an environment (Fig. 1B; Qian 2006).

This requirement can be verified for a simple and minimally realistic model of only 3 states linked by a closed loop of reactions, which represents a phosphorylation-dephosphorylation cycle for one protein interaction (Fig. 1B). Such a loop is the basic metabolic motif for modeling synaptic plasticity with multiple states, i.e., with many phosphorylation events (Fig. 1C). In this simple 3 state case, p_- denotes the probability of a protein in a ground state and p_+ is the probability of the activated protein (Fig. 1B). The protein can go from the state p_- to p_+ either directly, but it is rare and occurs with a small transition rate $\epsilon_1\alpha$ (where $\epsilon_1 \ll 1$), or it can go to the state p_+ indirectly, in two steps, through an intermediate state q_0 (by binding an enzymatic substrate). The interesting point is that this second step, from q_0 to p_+ can be very fast, with a large

transition rate a , depending on the level of protein phosphorylation that is powered by ATP hydrolysis. This simple 3 state protein is not in thermal equilibrium with its environment, because it continually transfer between the 3 states (p_- , q_0 , p_+), driven by energy provided by ATP. Therefore, this configuration dissipates energy even in the baseline, which can be found explicitly as entropy production rate EPR_0 at NESS (Fig. 1B)

$$\text{EPR}_0 = kT \frac{\alpha\beta}{Z} (\epsilon_2 a - \epsilon_1 \epsilon_3 b) \ln \left(\frac{\epsilon_2 a}{\epsilon_1 \epsilon_3 b} \right), \quad (1)$$

where Z is a function of different transition rates a, b, α, β , with ϵ_i unitless small coefficients ($\epsilon_i \ll 1$) (see Eq. 11 in Methods). The value of a is controlled directly by protein phosphorylation rate driven by ATP hydrolysis, and b is the dephosphorylation rate. The term $\epsilon_2 a - \epsilon_1 \epsilon_3 b$ represents the bias or deviation from thermal equilibrium, and corresponds to the probability flux (Eq. 9) that circulates between the three states. Eq. (1) implies that if the transitions do not form a loop, i.e. when $a = b = 0$, then $\text{EPR}_0 = 0$ (since $x \ln(x) \mapsto 0$ as $x \mapsto 0$). Moreover, to get a finite EPR_0 one needs bidirectional transitions. For unidirectional transitions, we obtain $\text{EPR}_0 \mapsto \infty$, as can be seen e.g. by setting $a > 0$ and $b = 0$. This obviously is unrealistic.

The steady state EPR_0 for the 3 state system (Fig. 1B) is also 0, when the condition of the so-called detailed balance is met, i.e., when the bias $\epsilon_2 a - \epsilon_1 \epsilon_3 b = 0$, which corresponds to thermodynamic equilibrium. The detailed balance can be broken (leading to nonequilibrium) if, e.g., ϵ_3 is much smaller than the rest of the parameters in Eq. (1).

This situation happens in a living cell, where there is a big asymmetry between phosphorylation and dephosphorylation, i.e. $a \gg \epsilon_3 b$ (Qian 2006). Generally, the higher that asymmetry the larger EPR_0 .

In the remaining of this study we investigate the metabolic constraints on learning an input and on its subsequent memory trace, in the model with multiple states (Fig. 1C).

Metabolic cost of baseline synaptic plasticity is insensitive on the number of synaptic states but it is affected by the transition rates between the states.

When synapses are not stimulated, their dynamics converge into baseline activity, which is the nonequilibrium steady state NESS with distributed occupancies of different states and multiple transition loops (Fig. 1C; Methods). All the transitions between these states are appropriately rescaled by a prefactor e^{-zk} to progressively slow down the downstream dynamics of the loops with the higher index k , where z is the slowing down factor. This prefactor is introduced to provide multiple time scales in the dynamics of intrasynaptic molecular interactions. In the NESS state in Fig. 1C, energy is constantly dissipated due to many phosphorylation-dephosphorylation loops, and this leads to nonzero basal synaptic metabolic rate. Entropy production rate EPR_0 associated with this state can be viewed as a metabolic cost of maintaining all the prior plasticity events, i.e., the memory of the past, and it is always greater than zero, and could be substantial even for one molecular pathway $\sim 0.5 \text{ kT/min}$ (Fig. 2). Generally, the baseline EPR_0 is essentially independent of the number of synaptic states n , but it depends on the magnitude of the transition rates between synaptic states (Fig. 2).

Specifically, increasing the rate of synaptic slowing down z makes EPR_0 monotonically smaller with a saturation for large z . On the other hand, EPR_0 as a function of ATP driven transitions with an amplitude a_0 exhibits more complicated shapes: either it increases up to a saturation with increasing a_0 for $z = 0$, or it has maxima for $z > 0$ (Fig. 2). These dependencies indicate that although the baseline NESS state requires some energy for its maintenance, its cost can be reduced by globally slowing the transitions between synapses (increasing z) and, simultaneously, by keeping the amplitude of ATP driven transitions (a_0) either very small or very large.

Stronger and longer synaptic stimulations lead to longer memory traces with higher energy expenditures, but with low relative costs.

Next, we study the energetics and the memory trace related to a single transient plasticity event. The plasticity event corresponds to synaptic stimulation by affecting all ATP-driven phosphorylation rates a_k^\pm associated with the transitions $q_k^\pm \leftrightarrow p_{k+1}^\pm$, which is a microscopic representation of some macroscopic learning (Fig. 1C). The stimulation is induced by a brief jump in the ATP-driven transition rates a_k^\pm , by a relative fraction $A_\pm(t) = A_\pm \exp(-t/\tau)$, which relaxes exponentially to zero with a time constant τ that can be also thought as a learning time. This perturbation leads to a redistribution of the occupancy probabilities of the synaptic states, and the recovery to the baseline probabilities takes some time, called memory lifetime T_m , which in general is much longer than the stimulation time τ .

The memory trace associated with the single stimulation is defined as the deviation of the average synaptic weight from its baseline value, relative to a noise in the weights.

This essentially corresponds to a signal-to-noise ratio SNR, which is given by Eqs. (12-14) in the Methods. Temporal dependences of memory trace SNR and synaptic energy rate EPR following a single stimulation are presented in Fig. 3. Upon stimulation from the NESS state, SNR initially builds up to some maximal value and then it slowly decays with a characteristic long tail, given by $\text{SNR} \sim t^{-\delta}$, where $\delta \approx 4/3$ (Fig. 3). Memory trace is detectable if SNR is above a certain threshold, which is taken here as 1 (the results are insensitive on the precise value of this threshold), and the corresponding memory lifetime T_m is defined as the time interval from the stimulation up to the moment when SNR drops below the threshold. Energy rate EPR associated with this stimulation has a qualitatively different time course than SNR, as it follows closely the temporal dependence of short-term stimulation $A_{\pm}(t)$, without exhibiting a long tail (Fig. 3). This means that EPR starts from a high level and quickly decays to its resting value EPR_0 when the stimulation ends (Fig. 3). Thus, most of the time when memory trace is still detectable, the energy rate is essentially at its resting value, which implies that the two variables decouple for longer times (Fig. 3). A direct consequence of this important observation is that the total energy E expanded on a new memory trace, defined as an area under EPR, differs in most cases only by a small percentage from a baseline energy E_0 ($E_0 = \text{EPR}_0 T_m$) required for supporting the baseline synaptic state related to all prior memories during time T_m (Fig. 4; see also below). This effect is much more pronounced for larger slowing down z , when the speed of downstream molecular reactions is severely reduced (Fig. 4). The relatively low energy cost is a sign of metabolic efficiency of a new memory storing in the cascade model of synaptic plasticity.

When longer memories require proportionally larger energy expenditure?

How the lifetime T_m of the memory trace and its energy cost E depend on the amplitude A_+ and duration τ of synaptic stimulation? Memory lifetime T_m generally increases with increasing A_+ and τ , but both dependences are roughly logarithmic (Fig. 5). The corresponding energy expenditure E on keeping the new memory trace SNR above the threshold also grows with A_+ and τ in a similar manner as T_m (Fig. 5). Interestingly, the energy cost E of a new memory increases in proportion to its lifetime T_m , as is evident by an approximate constancy of the ratio T_m/E over variability in the stimulus amplitude and its duration (Fig. 5). Moreover, the ratio T_m/E is larger for larger z , which implies that the gain in memory duration per invested energy is bigger if the rates of downstream molecular processes are reduced.

How general is the finding that energy cost of a memory trace increases proportionally with the memory lifetime? What happens if we keep the level of synaptic stimulation constant, and instead, change the intrinsic parameters characterizing synaptic plasticity? In Figs. (6-7) we show the dependence of T_m and an associated energy cost E on two internal synaptic parameters: basic number of synaptic states n , and the fraction of potentiated synapses f .

Increasing synaptic states n leads to an increase in T_m , but only for small n (Fig. 6). For larger n , the memory lifetime T_m saturates. The related energy cost E behaves similarly, such that E is proportional to T_m , which again follows from the observation that the ratio T_m/E does not change much over the whole range of n . A qualitatively similar pattern, with approximate constancy of T_m/E , is observed when the fraction of potentiated synapses f is changed (Fig. 7).

Taken together, in all these three cases a longer memory trace requires a proportionally more energy to sustain.

When longer memories do not require more energy?

A different picture emerges, regarding the relationship between E and T_m , when two other internal parameters are changed that are related to the speed of molecular transitions. One is the molecular slowing-down factor z , and another is the global amplitude of the phosphorylation rate a_0 .

Growing the parameter z leads to bimodal shapes of memory trace duration T_m and its energy cost E with the appearance of maxima (Fig. 8). In this case, however, the ratio T_m/E increases significantly with growing z , which indicates a substantial gain in memory duration per expanded energy (Fig. 8). This means that memory lifetime grows faster than its energy cost, i.e., longer memories are relatively cheaper. Interestingly, the ratio T_m/E is insensitive to the fraction of potentiated synapses f , as all dependencies collapse on a single line (Fig. 8).

A slightly more complex scenario appears when the ATP-driven phosphorylation amplitude a_0 is varied (Fig. 9). For $z = 0$, the memory lifetime T_m and energy E both increase monotonically with a_0 such that the ratio T_m/E initially decreases and then stabilizes at some level. For a more interesting case $z > 0$, the memory duration T_m and its cost E are not easily correlated: T_m initially grows and then saturates for larger a_0 , while the associated energy cost E always exhibits a maximum at some a_0 . More importantly, for $z > 0$, the ratio T_m/E displays a minimum, which is very close to the point where energy E has a maximum (Fig. 9). This means that there are two different

regimes: for small a_0 a relative cost of increasing memory lifetime strongly grows (sharp decrease in the ratio T_m/E), whereas for large a_0 the opposite happens and the relative cost of memory duration decreases (T_m/E increases). Thus, the latter regime is much more energy efficient, which is also visible in the high values of both T_m and T_m/E for large a_0 (Fig. 9).

Taken together, these two results suggest that storing longer memories is not always associated with a higher metabolic burden. In fact, there can be regimes in the internal synaptic parameters, here z and a_0 , for which longer memories can be relatively cheap.

Metabolic cost of a new memory relative to the cost of prior memories.

How expensive is to invoke a new plasticity event and keep its memory in the molecular interactions, relative to the cost of prior plasticity events “encoded” in the baseline spine metabolic rate? Figure 4 as well as lower panels of Figs. (6-9) provide an answer to this question. The relative cost of a new memory trace with respect to the baseline energy cost E_0 during T_m , i.e. the ratio $(E - E_0)/E_0$, is almost always smaller or much smaller than 1. Thus, the cost of keeping the new memory trace detectable is generally marginal to the cost of storing memories of all previous events.

DISCUSSION

Empirical metabolic efficiency of long-term synaptic plasticity.

Dendritic spines of excitatory synapses occupy only about 10% of neocortical volume of adult mammalian brain (Karbowski 2015), but their short-term signaling associated with fast synaptic transmission can cause a high metabolic burden to the whole cortex. Its estimated cost in the rat cortex is $8.4 \cdot 10^6$ ATP/min per spine (Attwell and Laughlin 2001), and the interesting question is how does it relate to the synaptic plasticity cost?

Proteins underlying molecular level of synaptic learning and memory constantly interact, which is associated with synaptic plasticity, and these processes require energy influx and thus some metabolic cost (Table 1). What is this overall cost, and to what extent it can constrain the memory trace? The empirical estimates conducted here suggest that the energy related to synaptic plasticity in rat cortex comprises only 4–11% of the energy used by excitatory synapses for fast synaptic transmission given above (Table 2). Considering that the latter energy (including all spines) constitutes around 30 – 80% of the total cortical metabolic rate (Attwell and Laughlin 2001; Harris et al 2012; Karbowski 2009 and 2012), we get that metabolic cost of learning and memory is only about 1 – 9% of the total metabolic rate. This is the empirical evidence that the processes of learning and information storing in synapses are energetically rather cheap.

What about the energetic constraints on memory trace? The cascade model considered here suggests that, although a longer memory trace requires proportionally larger amounts of energy (in most cases; Figs. 5–7), these amounts are relatively small (< 10%)

as compared to the baseline synaptic plasticity cost (Figs. 6-9).

Thus, it seems that synaptic plasticity is non-demanding metabolically in the scale of the whole brain, but nevertheless it can use a nontrivial part of the brain energy, which might in principle be detectable using imaging techniques (Logothetis 2008).

It should be also noted that the above low-cost percentages for synaptic plasticity agree qualitatively with the marginal role of protein synthesis and actin treadmilling in the metabolism of the whole brain (Rolfe and Brown 1997; Attwell and Laughlin 2001). Recent estimates in (Engl and Attwell 2015; Engl et al 2017) suggest however that actin treadmilling might be much more energy demanding, and overall that nonsignaling processes in the brain might require similar amounts of energy as those related to electric signaling (e.g. fast synaptic transmission). However, these estimates were made on data from brain slices, which may significantly differ from *in vivo* conditions. Additionally, they apply to the neurons as a whole, not specifically to synapses, as in this study. More importantly, Engl and Attwell (2015) and Engl et al (2017) consider nonsignaling processes, like lipid synthesis, microtubule turnover, and mitochondrial proton leak, which can be metabolically expensive, but which were not included in the present analysis for synaptic plasticity, primarily because they seem not to be directly related to plasticity processes.

The main reasons for the high metabolic efficiency of synaptic plasticity is the slowness of molecular processes and small number of molecules in spines related to learning and memory. For instance, protein synthesis is very slow with a mean time constant of about 3.7 days (Cohen et al 2013), which is orders of magnitude larger than the characteristic times associated with short-term synaptic signaling through AMPA and

NMDA receptors (respectively ~ 5 and 150 msec), and Na-K-ATPase pump activity (for pumping out Na^+ ions) operating on a time scale of a few seconds (Attwell and Laughlin 2001; Karbowski 2009). On the other hand, faster molecular processes associated with spine plasticity and related to activated protein phosphorylation, actin treadmilling and receptor trafficking, operating on a time scale from 0.1 – 1 sec to 20-40 sec (i.e. comparable or even faster to Na-K-ATPase) involve a relatively small number of molecules that are 2-3 orders of magnitude smaller than the number of Na^+ ions that have to be extruded following synaptic transmission. This high energy efficiency of memory on a molecular level is reminiscent of energy efficient sparse neural codes on a cellular level (Levy and Baxter 1996; Laughlin et al 1998).

Limitations of the empirical estimates.

Every estimation based on incomplete data is only approximate, and this is also the case for the above results based on molecular data. It seems that the greatest uncertainties are associated with the protein phosphorylation and plasticity modulation.

The rates of protein phosphorylation can vary by a factor of 10 for the active LTP phase. The precise values for each PSD protein are not known; at best we have some data for CaMKII, which fortunately is the most abundant protein in PSD (Sheng and Kim 2011). Additionally, the metabolic cost of phosphorylation depends on the fraction of proteins with elevated phosphorylation rates, which in turn depends on the presynaptic stimulation by Ca^{2+} influx. Based on limited data, we assumed that this fraction is about 10%. However, if it were 30% (under some conditions), then this would increase the overall cost of synaptic plasticity by a factor 3 to about 12 – 33% of the synaptic

transmission cost. The maximal possible value for the cost of synaptic plasticity was estimated above as $15 \cdot 10^6$ ATP/min, which means that in a hypothetical situation when all PSD proteins are maximally phosphorylated then the metabolic rate of synaptic plasticity is about twice of that for synaptic transmission. This value provides an upper bound on the theoretically possible cost of synaptic plasticity.

The cost of plasticity modulation is hard to compute exactly, as we are uncertain which pathways are affected and to what extent. We took only one of the possible ways of modulation (through P2X receptors), and even for this case we do not have numerical values of the transition rates modulation. The modulation cost was deduced based on the “end product”, i.e., the extent to which the synaptic weight can change.

Cascade model with phosphorylation cycles reveals metabolic efficiency of synaptic memory.

The main theoretical findings of this study are as follows. (i) There is a nonzero cost of storing all previous plasticity events, i.e. prior memory, which is kept in baseline entropy production rate EPR_0 (Figs. 2 and 3). (ii) In most cases, the metabolic cost of a new learning and its memory trace increases proportionally with memory duration, such that their ratio is essentially constant (Figs. 5-7). (iii) A different trend is observed for the two key parameters, slowing down factor z and ATP driven transition amplitude a_0 , for which a memory lifetime per expanded energy grows for longer memories (Figs. 8 and 9). (iv) Memory trace decays with time as a power law, while the associated with it metabolic rate decays to its baseline much faster, exponentially, which leads to the dynamic decoupling of memory trace and its metabolism (Fig. 3). The likely reason for

the fast decay of the metabolic rate is that EPR depends nonlinearly on the probabilities and transition rates. (v) The direct consequence of (iv) is that maintenance of a new memory takes only a small fraction of the energy required for the baseline synaptic state, i.e. the ratio $\Delta E/E_0 \ll 1$ (Figs. 6-9). Additionally, the huge majority of energy is expanded during the learning phase (synaptic stimulation), and the memory phase (after the stimulation) is relatively costless (Fig. 3).

Points (ii) and (iii) indicate that while there is some cost to learning and storing a new memory, it can be minimized if the right parameters are appropriately tuned. Points (iv) and (v) indicate that memory trace and its metabolic energy consumption are governed by different dynamical time scales and are essentially independent for long times, which leads to a relatively low cost of a new memory. Both effects are more pronounced if the slowing down factor z is large, which indicates that the diversity of time scales associated with biochemical synaptic cascades increases not only the memory lifetime (Fusi et al 2005; Benna and Fusi 2016), but also enhances its metabolic efficiency. Even bigger metabolic efficiency is obtained if the ATP driven phosphorylation amplitude a_0 is made larger (Fig. 9). Surprisingly, in this case it is possible to have longer memories for less energy if a_0 and z are sufficiently large.

How can we explain the effects of a_0 and z on the energetic efficiency of memory? They can be explained by noting that increasing z causes decreasing the speed of all molecular processes that in turn consume less energy per time unit (Fig. 2, middle panel). Additionally, the resting metabolic rate EPR_0 depends non-monotonically on a_0 for $z > 0$, and generally EPR_0 decreases with increasing a_0 if a_0 is large (Fig. 2, bottom panel). In this case the ratio T_m/E has a minimum for some a_0 if $z > 0$

(Fig. 9), but then T_m/E generally steady increases for large a_0 , suggesting an enhanced metabolic efficiency of synaptic memory in this regime.

It should be noted that the energy cost of a new learning and its memory trace found here is a theoretical minimum, because the cascade model considers only protein phosphorylation. Inclusion of the other energy consuming molecular processes would be much more complicated and would require a much more complex model that goes far beyond simple Markov models analyzed within a Master equation approach.

Model of synaptic plasticity as phosphorylation cascades.

The cascade model of synaptic plasticity presented in this study differs from the previous cascade models (Fusi et al 2005; Leibold and Kempter 2008; Barrett et al 2009; Benna and Fusi 2016). First, the transitions between synaptic states are bidirectional here, as opposed to the majority of the previous models (see however, Benna and Fusi 2016, as an exception). Second, the present model contains many local cyclic motifs, corresponding to ATP driven protein phosphorylation, which are absent in the previous models. Strictly speaking, there are some loops in the topology of the previous models but they are unidirectional and non local, and hence it is difficult to interpret their physical meaning. Third, and most importantly, the current study ask a fundamentally different question, namely the energy cost and efficiency of memory on a spine level. It should be stressed that, without bidirectional cyclic motifs, most of the previous cascade models are inappropriate for studying metabolic constraints on memory, since they are thermodynamically inconsistent and produce singular entropy production rate (metabolic rate), as explained in this study (Qian 2006, 2007).

These differences generate also qualitative differences in some results. For instance, the signal to noise memory trace SNR decays here for long times as $\sim t^{-4/3}$ (Fig. 3), which is much faster than in Benna and Fusi (2016), where it decays as $\sim t^{-1/2}$. The primary reason for this is that the Benna and Fusi (2016) model is optimized, while the current model is not. Another difference is that here the memory lifetime always saturates (Figs. 5-9), also as a function of the number of basic states n (Fig. 6). In contrast, in the Benna and Fusi (2016) model the memory duration increases exponentially with synaptic complexity, which may be equivalent to n . The likely explanation for this difference is the presence of many local cycles in the structure of the current model, which provide additional pathways for faster relaxation to baseline conditions.

Limitations of the present model.

The model presented in this study is an obvious simplification of a much more complicated web of molecular interactions in a typical spine. However, the goal here was not to model the spine in its full complexity, but rather to identify key parameters related to energy consumption during memory storage that are most sensitive in terms of metabolic efficiency, and this could be best done for simple models. Nevertheless, the current model can be modified and extended by including specific molecular details, such as those considered in several previous studies (Miller et al 2005; Hayer and Bhalla 2005; Graupner and Brunel 2007; Bhalla 2011; Antunes and Schutter 2012; Smolen et al 2012; Kim et al 2013).

Implications of energy efficient memory storage.

The empirical estimates as well as the theoretical analysis performed here imply that molecular storing of memory can be relatively cheap under some conditions ($\leq 11\%$ of the synaptic transmission cost). This result can have important implications for building energy efficient artificial silicon systems that mimic brain function by storing and processing information (Esser et al 2016; Sun et al 2018). The key here is to have bidirectional loops in the topology of subsynaptic biochemical pathways with appropriately tuned transition rates and multiple time constants, not only to prevent catastrophic forgetting in neural networks (Kirkpatrick et al 2017) but also to spend small amounts of energy on long-term synaptic computations.

Another potential implication of the current results is for biomedical research related to neurodevelopmental disorders. There are experimental data showing a close relationship between phosphorylation signaling in PSD and diseases such as schizophrenia and autism (Li et al 2016). Interestingly, many genes encoding PSD overlap with mutated genes responsible for schizophrenia and for autistic phenotype (De Rubeis et al 2014; Iossifov et al 2014; Fromer et al 2014; Kaizuka and Takumi 2018). In the light of the results obtained in this study, it is not difficult to understand this close relationship given the easiness with which one can alter memory lifetime and its energetic efficiency by manipulating transition rates related to ATP driven protein phosphorylation. Moreover, there are many empirical studies showing that increased glucose metabolism can enhance memory in mammals, which is known as “glucose memory facilitation effect”, in a dose-dependent fashion (Gold 2005; Smith et al 2011). The latter means that some glucose levels can facilitate memory, while others can be neutral or even detrimental

for memory. Using our model, this phenomenon can be understood by noting that ATP that drives protein phosphorylation is generated directly by glucose (Rolfe and Brown 1997). This means that glucose metabolic rates can affect ATP rates used for powering spine PSD proteins and downstream molecular processes related to synaptic information storing, e.g. as shown in Fig. (9).

METHODS

Cascade model of synaptic plasticity with bidirectional cycles.

We model biochemical processes underlying synaptic plasticity in a dendritic spine as transitions between discrete synaptic states (Montgomery and Madison 2004), which describe various levels of protein activation in spine PSD (Fig. 1). The model of plasticity considered here is a generalization of previous models of cascade synaptic plasticity (Fusi et al 2005) and is treated as a Master Equation system (Schnakenberg 1976). The main modification in the current approach is the addition of closed loops or cycles with bidirectional transitions between different states, corresponding to protein phosphorylation (Qian 2006).

A synapse can be in one of many “down” and “up” states corresponding to biochemical process associated with LTD and LTP, respectively (Fig. 1). There are n basic up states and n basic down states, whose probabilities of occupancy are given by p_k^+ and p_k^- , respectively for $k = 1, \dots, n$. There are two types of transitions between neighboring p_k^\pm states: direct spontaneous transitions driven by thermal fluctuations (with transition rates α_k^\pm and $\epsilon_1 \alpha_k^\pm$), and indirect transitions that contain ATP driven reactions (with transition rates a_k^\pm and $\epsilon_3 b$) and non-ATP reactions (with transition rates β_k^\pm and $\epsilon_2 \beta_k^\pm$). The direct transitions are rare, while the indirect ones can be massive if the synapse is electrically stimulated in a way that induces plasticity mechanisms (LTP and LTD), and elevation of local ATP concentration. Additionally, the ATP related transitions require intermediate states with probabilities of occupancy q_k^\pm , which describe metastable states with proteins ready for phosphorylation (for details see, e.g., Qian 2007). Each

loop or cyclic motif represented by transitions $p_k^\pm \mapsto q_k^\pm \mapsto p_{k+1}^\pm \mapsto p_k^\pm$, can be thought as a cascading phosphorylation of various downstream proteins in spine PSD.

It is also assumed that the dynamics of downstream cascades are progressively slower, similar to the previous models (Fusi et al 2005; Benna and Fusi 2016). Mathematically, this is implemented by a prefactor $g_k = \exp(-zk)$, which rescales all the transition rates and gets smaller for deeper states with higher index k , where z is the slowing down factor.

The dynamics of state probabilities are given by

$$\begin{aligned}\dot{p}_k^\pm &= g_{k-1}(\epsilon_1 \alpha_{k-1}^\pm p_{k-1}^\pm + a_{k-1}^\pm q_{k-1}^\pm) + g_k(\alpha_k^\pm p_{k+1}^\pm + \beta_k^\pm q_k^\pm) \\ &\quad - [g_{k-1}(\epsilon_3 b_0 + \alpha_{k-1}^\pm) + g_k(\epsilon_1 \alpha_k^\pm + \epsilon_2 \beta_k^\pm)] p_k^\pm\end{aligned}\tag{2}$$

for $2 \leq k \leq n-1$, where the dot denotes the time derivative. For $k = n$ we have

$$\dot{p}_n^\pm = g_{n-1} \left(a_{n-1}^\pm q_{n-1}^\pm + \epsilon_1 \alpha_{n-1}^\pm p_{n-1}^\pm - (\epsilon_3 b_0 + \alpha_{n-1}^\pm) p_n^\pm \right), \tag{3}$$

and for $k = 1$ we have

$$\begin{aligned}\dot{p}_1^+ &= \epsilon_1 \alpha_0 p_1^- + a_0 q_0 + g_1(\alpha_1^+ p_2^+ + \beta_1^+ q_1^+) \\ &\quad - [g_1(\epsilon_1 \alpha_1^+ + \epsilon_2 \beta_1^+) + \alpha_0 + \epsilon_3 b_0] p_1^+\end{aligned}\tag{4}$$

and

$$\begin{aligned}\dot{p}_1^- &= \alpha_0 p_1^+ + \beta_0 q_0 + g_1(\alpha_1^- p_2^- + \beta_1^- q_1^-) \\ &\quad - [g_1(\epsilon_1 \alpha_1^- + \epsilon_2 \beta_1^-) + \epsilon_1 \alpha_0 + \epsilon_2 \beta_0] p_1^-.\end{aligned}\tag{5}$$

The dynamics of the intermediate states involved in protein phosphorylation are given by

$$\dot{q}_k^\pm = g_k \left(\epsilon_2 \beta_k^\pm p_k^\pm + \epsilon_3 b_0 p_{k+1}^\pm - (a_k^\pm + \beta_k^\pm) q_k^\pm \right), \tag{6}$$

for $1 \leq k \leq n$, and

$$\dot{q}_0 = \epsilon_2 \beta_0 p_1^- + \epsilon_3 b_0 p_1^+ - (a_0 + \beta_0) q_0. \tag{7}$$

The transition rates $\alpha_k^\pm, \beta_k^\pm, a_k^\pm$ are heterogeneous across different cycles and given by $\alpha_k^\pm = \alpha_0(1 + \sigma \eta_k^\pm)$, $\beta_k^\pm = \beta_0(1 + \sigma \eta_k^\pm)$, and $a_k^\pm = a_0(1 + \sigma \eta_k^\pm)$, where η_k^\pm are random variables uniformly distributed between -1 and 1 , and σ is a measure of heterogeneity ($0 \leq \sigma < 1$). The parameters α_0, β_0 , and a_0 are the amplitudes of the above transition rates. When the synapses are stimulated, only the ATP-driven rates a_k^\pm, a_0 are time dependent (see below).

Let us consider two examples of 3 state models: one with a ladder structure (Fig.

1A), and another with a loop structure (Fig. 1B). For the ladder structure (Fig. 1A) we have the dynamics of state probabilities p_1, p_2, p_3 as

$$\begin{aligned}\dot{p}_1 &= J_{12}, \\ \dot{p}_2 &= J_{21} - J_{32}, \\ \dot{p}_3 &= J_{32},\end{aligned}\tag{8}$$

where the probability fluxes are defined as: $J_{12} = w_{12}p_2 - w_{21}p_1$ (flux from state 2 to state 1), $J_{32} = w_{32}p_2 - w_{23}p_3$ (flux from state 2 to state 3), $J_{21} = -J_{12}$ (flux from state 1 to state 2). At the steady-state ($\dot{p}_1 = \dot{p}_2 = \dot{p}_3 = 0$), we obtain $w_{12}p_2 = w_{21}p_1$, and $w_{32}p_2 = w_{23}p_3$. From this it follows that all steady-state fluxes $J_{12} = J_{32} = 0$, which is known as the condition of the detailed balance (Lebowitz and Spohn 1999; Mehta and Schwab 2012).

For the second example with a loop (Fig. 1B), the dynamics of state probabilities p_+, p_-, q_0 read:

$$\begin{aligned}\dot{p}_+ &= J_{+0} + J_{+-}, \\ \dot{p}_- &= J_{-0} - J_{+-}, \\ \dot{q}_0 &= -J_{+0} - J_{-0},\end{aligned}\tag{9}$$

where the probability fluxes are defined as: $J_{+0} = aq_0 - \epsilon_3 b p_+$ (flux from state 0 to +),

$J_{+-} = \epsilon_1 \alpha p_- - \alpha p_+$ (flux from state $-$ to $+$), $J_{-0} = \beta q_0 - \epsilon_2 \beta p_-$ (flux from state 0 to $-$), and the opposite fluxes are $J_{0+} = -J_{+0}$, $J_{-+} = -J_{+-}$, and $J_{0-} = -J_{-0}$. For this cyclic motif, we can find steady-state values of the probabilities as:

$$\begin{aligned} p_+ &= Z^{-1} [\epsilon_1 \alpha (a + \beta) + \epsilon_2 a \beta], \\ p_- &= Z^{-1} [\alpha (a + \beta) + \epsilon_3 b \beta], \\ q_0 &= Z^{-1} [\epsilon_2 \alpha \beta + \epsilon_3 (\epsilon_1 \alpha + \epsilon_2 \beta)], \end{aligned} \quad (10)$$

where Z is given by

$$Z = \alpha[(1 + \epsilon_1 + \epsilon_2)\beta + (1 + \epsilon_1)a + \epsilon_1 \epsilon_3 b] + \beta[\epsilon_2 a + \epsilon_3(1 + \epsilon_2)b]. \quad (11)$$

At the steady-state the above fluxes must balance each other, i.e., $J_{+0} = -J_{+-} = -J_{-0} \equiv J$, where the emerging flux $J = \alpha \beta Z^{-1}(\epsilon_1 \epsilon_3 b - \epsilon_2 a)$. Note that the flux J is generally nonzero, which is a signature of a nonequilibrium steady-state, denoted as NESS (Lebowitz and Spohn 1999; Bustamante et al 2005; Van den Broeck and Esposito 2015). It vanishes only if the phosphorylation and dephosphorylation rates (a and $\epsilon_3 b$) are both zero (cyclic motif is destroyed), or for the special case of the so-called detailed balance when $\epsilon_1 \epsilon_3 b = \epsilon_2 a$. The latter two situations correspond to thermodynamic equilibrium when neither energy nor material is exchanged with the environment (“thermodynamic death”, e.g., Nicolis and Prigogine 1977).

Memory trace and signal to noise ratio.

We consider N_s independent synapses for which we first determine their non-equilibrium steady-state NESS. This is done by starting from uniform initial conditions for the state probabilities p_k^\pm, q_k^\pm and allowing them to relax to the baseline state denoted as $p_{k,\infty}^\pm, q_{k,\infty}^\pm$. A next phase is a brief stimulation of synapses from their baseline and observation of the associated memory lifetime of this event. During the stimulation and subsequent memory decay, the synapses are divided into two populations: the fraction f of synapses undergoes LTP process, and the remaining $1 - f$ synapses perform LTD process. The LTP synapses are stimulated by a pulse in the ATP-driven transitions a_0, a_k^+ , while the LTD synapses are activated by a pulse in the ATP-driven transitions a_k^- , with the explicit time dependences given by $a_k^\pm(t) = a_k^\pm[1 + A_\pm \exp(-t/\tau)]$ for $k > 1$, and $a_0(t) = a_0[1 + A_+ \exp(-t/\tau)]$, where τ is the characteristic time of stimulation, and t is the time counted from the onset of stimulation. We assume that $A_+ > A_-$, which reflects an experimental fact that LTP (LTD) is induced by high (low) frequency stimulation.

We assume that all down states (including q_0) have the same synaptic efficacy (weight) w , and all up states have the same efficacy $2w$, where w is the synaptic conductance. (Its value is irrelevant for the results of this study.) This binary choice is consistent with neurophysiological data (Petersen et al 1998; O'Connor et al 2005). Thus, the probability that a randomly chosen synapse undergoes LTD and has weight w is $(1-f)(p_{LTD}^- + q_{LTD}^-)$, and the probability that it has weight $2w$ is $(1-f)(p_{LTD}^+ + q_{LTD}^+)$, where $p_{LTD}^\pm = \sum_k p_{k,LTD}^\pm$, and $q_{LTD}^\pm = \sum_k q_{k,LTD}^\pm$. Similarly, the probability that a randomly selected synapse undergoes LTP and has weight w is $f(p_{LTP}^- + q_{LTP}^-)$, and that it

has weight $2w$ is $f(p_{LTP}^+ + q_{LTP}^+)$, where $p_{LTP}^\pm = \sum_k p_{k,LTP}^\pm$, and $q_{LTP}^\pm = \sum_k q_{k,LTP}^\pm + q_0$. From this it follows that the average synaptic weight $\langle V \rangle$ for the whole synaptic population is given by

$$\begin{aligned} \langle V \rangle = w & \left[(1-f)(p_{LTD}^- + q_{LTD}^-) + f(p_{LTP}^- + q_{LTP}^-) \right] \\ & + 2w \left[(1-f)(p_{LTD}^+ + q_{LTD}^+) + f(p_{LTP}^+ + q_{LTP}^+) \right]. \end{aligned} \quad (12)$$

Consequently, the variance in a population synaptic weight, i.e. $\langle V^2 \rangle - \langle V \rangle^2$, is

$$\begin{aligned} \langle V^2 \rangle - \langle V \rangle^2 = w^2 & \left[(1-f)(p_{LTD}^- + q_{LTD}^-) + f(p_{LTP}^- + q_{LTP}^-) \right] \\ & \times \left[(1-f)(p_{LTD}^+ + q_{LTD}^+) + f(p_{LTP}^+ + q_{LTP}^+) \right]. \end{aligned} \quad (13)$$

We define a synaptic memory trace as a deviation of the average synaptic weight $\langle V \rangle$ from its baseline value $\langle V \rangle_b$, and normalized by a standard deviation in V (similar to Fusi et al 2005). This is equivalent to the definition of signal to noise ratio SNR at time t :

$$\text{SNR}(t) = \sqrt{N_s} \frac{(\langle V \rangle - \langle V \rangle_b)}{\sqrt{\langle V^2 \rangle - \langle V \rangle^2}}, \quad (14)$$

where the prefactor $\sqrt{N_s}$ comes from summing contributions from all the synapses in a

small cortical region. Note that after a synaptic stimulation both, the signal $\langle V \rangle$ and the variance in the denominator, are time dependent. Note also that SNR does not depend on the value of synaptic weight w (it cancels out). It is assumed that when SNR drops below a value of 1, the memory trace becomes undetectable and this time determines the memory lifetime T_m . The general results and conclusions are independent of the precise choice of this threshold.

Entropy production as a synaptic metabolic rate.

Metabolic rate (or the rate of dissipated energy) associated with cascading biochemical processes in a synapse is associated with entropy production rate EPR, which is defined as (Schnakenberg 1976; Lebowitz and Spohn 1999; Van den Broeck and Esposito 2015)

$$\text{EPR} = \frac{1}{2}kT \sum_{i,j} (w_{ij}P_j - w_{ji}P_i) \ln \frac{w_{ij}P_j}{w_{ji}P_i} \quad (15)$$

where k is the Boltzmann constant and T the brain temperature, w_{ij} are the transition rates between states j and i , and P_i is the probability of the state i occupancy. The above EPR should be understood as an energy rate per a single biochemical cascade; in the case of many cascades, the result should be multiplied by the number of pathways. Note that when the transition between two given states is unidirectional, then one of transition rates in a pair (either w_{ij} or w_{ji}) must vanish. This means that a corresponding logarithm in the sum must diverge to infinity, which implies a divergent metabolic rate. This is clearly not a realistic description of the energetics of any

biological system, which suggests that one must always keep all the transition rates as bidirectional (regardless of how small they are). Unfortunately, this important fact was overlooked in early models of cascade plasticity, where many transitions were chosen as unidirectional (Fusi et al 2005; Leibold and Kempter 2008; Barrett et al 2009), and only recently it was realized that bidirectionality is important for a memory lifetime duration (Benna and Fusi 2016).

In a particular case of a simple 3 state model with a ladder structure (Fig. 1A), the entropy production rate at steady-state is zero. This is due to the detailed balance condition $w_{12}p_2 = w_{21}p_1$ and $w_{32}p_2 = w_{23}p_3$, which implies that all the terms in Eq. (15) are zero. This situation corresponds to a vanishing flux, which means that our 3 state system at steady state is in thermal equilibrium with its environment.

On the contrary, for the 3 state model with a loop (Fig. 1B), the detailed balance is broken, and there is a circulating flux even at steady-state, which leads to a non zero EPR given by Eq. (1).

For our plasticity model with $2n - 1$ basic cyclic motifs (Fig. 1C), EPR has five major contributions: two caused by direct transitions within down states (EPR_{pp}^-) and within up states (EPR_{pp}^+), two contributions caused by indirect transitions involving p and q states either for down (EPR_{pq}^-) or for up states (EPR_{pq}^+), and one contribution related to transitions within the basic loop $p_1^- \mapsto p_1^+ \mapsto q_0 \mapsto p_1^-$ (EPR_{ppq}). Thus, the EPR associated with synaptic plasticity takes the form

$$\text{EPR} = \text{EPR}_{pp}^- + \text{EPR}_{pp}^+ + \text{EPR}_{pq}^- + \text{EPR}_{pq}^+ + \text{EPR}_{ppq}, \quad (16)$$

where the appropriate contributions read

$$\text{EPR}_{pp}^{\pm} = \sum_{k=1}^{n-1} g_k \alpha_k^{\pm} (\epsilon_1 p_k^{\pm} - p_{k+1}^{\pm}) \ln \left(\frac{\epsilon_1 p_k^{\pm}}{p_{k+1}^{\pm}} \right), \quad (17)$$

$$\text{EPR}_{pq}^{\pm} = \sum_{k=1}^{n-1} g_k \left[\beta_k^{\pm} (\epsilon_2 p_k^{\pm} - q_k^{\pm}) \ln \left(\frac{\epsilon_2 p_k^{\pm}}{q_k^{\pm}} \right) + (\epsilon_3 b_0 p_{k+1}^{\pm} - a_k^{\pm} q_k^{\pm}) \ln \left(\frac{\epsilon_3 b_0 p_{k+1}^{\pm}}{a_k^{\pm} q_k^{\pm}} \right) \right], \quad (18)$$

and the basic loop contribution is

$$\begin{aligned} \text{EPR}_{ppq} = & \alpha_0 (p_1^+ - \epsilon_1 p_1^-) \ln \left(\frac{p_1^+}{\epsilon_1 p_1^-} \right) + \beta_0 (q_0 - \epsilon_2 p_1^-) \ln \left(\frac{q_0}{\epsilon_2 p_1^-} \right) \\ & + (a_0 q_0 - \epsilon_3 b_0 p_1^+) \ln \left(\frac{a_0 q_0}{\epsilon_3 b_0 p_1^+} \right). \end{aligned} \quad (19)$$

Energy used for synaptic stimulation and subsequent recovery to NESS state, which is the energy needed to keep a memory trace above the threshold is defined as

$$E = \int_0^{T_m} dt \text{ EPR}(t), \quad (20)$$

where $t = 0$ relates to the moment of stimulation. The relative energy used for maintaining memory is defined as the ratio $(E - E_0)/E_0$, where $E_0 = \text{EPR}_0 T_m$ is the baseline energy used during the time interval of duration T_m , and EPR_0 is the baseline entropy production rate.

Parameters used in the model.

The following default values of the parameters were used. For the transition rates: $a_0 = 0.4 \text{ min}^{-1}$, $b_0 = 0.2 \text{ min}^{-1}$ (Molden et al 2014), $\alpha_0 = 0.05 \text{ min}^{-1}$, $\beta_0 = 20.0 \text{ min}^{-1}$ (Miller et al 2005), $\epsilon_1 = 0.001$, $\epsilon_2 = 0.05$, $\epsilon_3 = 0.0001$ (there is high asymmetry between reaction rates for protein phosphorylation and dephosphorylation, see Qian 2006 and 2007), $\sigma = 0.25$. Note that the direct spontaneous transitions for protein activation induced by thermal fluctuations are much weaker than intermediate transitions associated with ATP hydrolysis. Default values for synaptic stimulation: $A_+ = 50$, $A_- = 10$, and $\tau = 10 \text{ min}$. Other values: number of synapses $N_s = 10^7$ (typical number in a cortical column with 10^3 neurons), number of states for up and down configurations $n = 5$, fraction of potentiated synapses $f = 0.5$, and the slowing-down rate $z = 0.8$. All the figures are made for these default values unless indicated otherwise.

Acknowledgments

The work was supported by the Polish National Science Centre (NCN) grant no. 2015/17/B/NZ4/02600.

Declaration of interests

The author declares no competing interests.

References

Abraham WC, Bear MF (1996) Metaplasticity: the plasticity of synaptic plasticity. *Trends Neurosci.* **19**: 126-130.

Aiello LC, Wheeler P (1995) The expensive-tissue hypothesis: The brain and the digestive-system in human and primate evolution. *Curr. Anthropology* **36**: 199-221.

Antunes G, Schutter ED (2012) A stochastic signaling network mediates the probabilistic induction of cerebellar long-term depression. *J. Neurosci.* **32**: 9288-9300.

Attwell D, Laughlin SB (2001) An energy budget for signaling in the gray matter of the brain. *J. Cereb. Blood Flow Metabol.* **21**: 1133-1145.

Barrett AB, Billings GO, Morris RGM, van Rossum MCW (2009) State based model of long-term potentiation and synaptic tagging and capture. *PLoS Comput. Biol.* **5**: e1000259.

Bayes A, Collins MO, Croning MD, van de Lagemaat LN, Choudhary JS, Grant SG (2012) Comparative study of human and mouse postsynaptic proteomes finds high compositional conservation and abundance differences for key synaptic proteins. *PLoS ONE* **7**: e46683.

Bean BP, Williams CA, Ceelen PW (1990) ATP-activated channels in rat and bullfrog sensory neurons: current-voltage relation and single-channel behavior. *J. Neurosci.* **10**: 11-19.

Benna MK, Fusi S (2016) Computational principles of synaptic memory consolidation. *Nature Neurosci.* **19**: 1697-1706.

Bhalla US (2011) Trafficking motifs as the basis for two-compartment signaling systems to form multiple stable states. *Biophys. J.* **101**: 21-32.

Bhalla US, Iyengar R (1999) Emergent properties of networks of biological signaling pathways. *Science* **283**: 381-387.

Bhalla US (2014) Molecular computation in neurons: a modeling perspective. *Curr. Opin. Neurobiol.* **25**: 31-37.

Bosch M, Castro J, Saneyoshi T, Matsuno H, Sur M, Hayashi Y (2014) Structural and molecular remodeling of dendritic spine substructures during long-term potentiation. *Neuron* **82**: 444-459.

Borgdorff AJ, Choquet D (2002) Regulation of AMPA receptor lateral movements. *Nature* **417**: 649-653.

Bradshaw JM, Hudmon A, Schulman H (2002) Chemical quenched flow kinetic studies indicate an intraholoenzyme autophosphorylation mechanism for Ca^{2+} /Calmodulin-dependent protein kinase II. *J. Biol. Chem.* **277**: 20991-20998.

Bustamante C, Liphardt J, Ritort F (2005) The nonequilibrium thermodynamics of small systems. *Phys. Today* **58**: 43.

Chaudhuri R, Fiete I (2016) Computational principles of memory. *Nature Neurosci.* **19**: 394-403.

Chen X, Vinade L, Leapman RD, Petersen JD, Nakagawa T, Phillips TM, Sheng M, Reese TS (2005) Mass of the postsynaptic density and enumeration of three key molecules. *Proc. Natl. Acad. Sci. USA* **102**: 11551-11556.

Choquet D, Triller A (2013) The dynamic synapse. *Neuron* **80**: 691-703.

Cingolani LA, Goda Y (2008) Actin in action: the interplay between the actin cytoskeleton and synaptic efficacy. *Nat. Rev. Neurosci.* **9**: 344-356.

Clarke DD, Sokoloff L (1994) In Siegel GJ et al (eds), *Basic Neurochemistry*, pp. 645-

680. Raven: New York, NY.

Coba MP, Pocklington AJ, Collins MO, Kopanitsa MV, Uren RT, Swamy S, Croning MD, Choudhary JS, Grant SG (2009) Neurotransmitters drive combinatorial multistate postsynaptic density networks. *Sci. Signal.* **2**: ra19.

Cohen LD, Zuchman R, Sorokina O, Muller A, Dieterich DC, Armstrong JD, et al. (2013) Metabolic turnover of synaptic proteins: kinetics, interdependencies and implications for synaptic maintenance. *PLoS ONE* **8**: e63191.

Colbran RJ (1993) Inactivation of Ca^{2+} /Calmodulin-dependent protein kinase II by basal autophosphorylation. *J. Biol. Chem.* **268**: 7163-7170.

Collins MO, Yu L, Coba MP, Husi H, Campuzano I, Blackstock WP, Choudhary JS, Grant SCN (2005) Proteomic analysis of in vivo phosphorylated synaptic proteins. *J. Biol. Chem.* **280**: 5972-5982.

De Koninck P, Schulman H (1998) Sensitivity of CaM kinase II to the frequency of Ca^{2+} oscillations. *Science* **279**: 227-230.

De Rubeis S, He X, Goldberg AP, Poultney CS, Samocha K, et al (2014) Synaptic, transcriptional and chromatin genes disrupted in autism. *Nature* **515**: 209-215.

Devineni N, Minamide LS, Niu M, Safer D, Verma R, Bamburg JR, Nachmias VT (1999) A quantitative analysis of G-actin binding proteins and the G-actin pool in developing chick brain. *Brain Res.* **823**: 129-140.

Ehlers MD (2000) Reinsertion or degradation of AMPA receptors determined by activity-dependent endocytic sorting. *Neuron* **28**: 511-525.

Engl E, Attwell D (2015) Non-signalling energy use in the brain. *J. Physiol.* **593**: 3417-3429.

Engl E, Jolivet R, Hall CN, Attwell D (2017) Non-signalling energy use in the developing rat brain. *J. Cereb. Blood Flow Metab.* **37**: 951-966.

Esser SK, Merolla PA, Arthur JV, Cassidy AS, Appuswamy R et al (2016) Convolutional networks for fast, energy-efficient neuromorphic computing. *Proc. Natl. Acad. Sci. USA* **113**: 11441-11446.

Fanselow EE, Nicolelis MAL (1999) Behavioral modulation of tactile responses in the rat somatosensory system. *J. Neurosci.* **19**: 7603-7616.

Francois-Martin C, Rothman JE, Pincet F (2017) Low energy cost for optimal speed and control of membrane fusion. *Proc. Natl. Acad. Sci. USA* **114**: 1238-1241.

Fromer M, Pocklington AJ, Kavanagh DH, Williams HJ, Dwyer S, et al (2014) De novo mutations in schizophrenia implicate synaptic networks. *Nature* **506**: 179-184.

Fusi S, Drew PJ, Abbott LF (2005) Cascade models of synaptically stored memories. *Neuron* **45**: 599-611.

Gaertner TR, Kolodziej SJ, Wang D, Kobayashi R, et al (2004) Comparative analyses of the three-dimensional structures and enzymatic properties of α , β , γ and δ isoforms of Ca^{2+} -Calmodulin-dependent protein kinase II. *J. Biol. Chem.* **279**: 12484-12494.

Gold PE (2005) Glucose and age-related changes in memory. *Neurobiol. Aging* **26S**: S60-S64.

Gordon GRJ, Baimoukhametova DV, Hewitt SA, Kosala WRA, Rajapaksha JS, Fisher TE, Bains J (2005) Norepinephrine triggers release of glial ATP to increase postsynaptic efficacy. *Nat. Neurosci.* **8**: 1078-1086.

Grafmuller A, Shillcock J, Lipowsky R (2009) The fusion of membranes and vesicles: pathway and energy barriers from dissipative particle dynamics. *Biophys. J* **96**: 2658-

2675.

Graupner M, Brunel N (2007) STDP in a bistable synapse model based on CaMKII switch: dependence on the number of enzyme molecules and protein turnover. *PLoS Comput. Biol.* **3**: e221.

Gumbart J, Chipot C, Schulten K (2011) Free-energy cost for translocon-assisted insertion of membrane proteins. *Proc. Natl. Acad. Sci. USA* **108**: 3596-3601. Harris JJ, Jolivet R, Attwell D (2012) Synaptic energy use and supply. *Neuron* **75**: 762-777.

Hayer A, Bhalla US (2005) Molecular switches at the synapse emerge from receptor and kinase traffic. *PLoS Comput. Biol.* **1**: e20.

Hill TL (1989) *Free Energy Transduction and Biochemical Cycle Kinetics*. New York: Springer-Verlag.

Honkura N, Matsuzaki M, Noguchi J, Ellis-Davies GCR, Kasai H (2008) The subspine organization of actin fibers regulates the structure and plasticity of dendritic spines. *Neuron* **57**: 719-729.

Huganir RL, Nicoll RA (2013) AMPARs and synaptic plasticity: the last 25 years. *Neuron* **80**: 704-717.

Iossifov I, O'Roak BJ, Sanders SJ, Ronemus M, Krumm N, et al (2014) The contribution of de novo coding mutations to autism spectrum disorder. *Nature* **515**: 216-221.

Jourdain P, Bergersen LH, Bhaukaurally K, et al (2007) Glutamate exocytosis from astrocytes controls synaptic strength. *Nat. Neurosci.* **10**: 331-339.

Kaizuka T, Takumi T (2018) Postsynaptic density proteins and their involvement in neurodevelopmental disorders. *J. Biochem.* **163**: 447-455.

Kandel ER, Dudai Y, Mayford MR (2014) The molecular and systems biology of mem-

ory. *Cell* **157**: 163-186.

Karbowski J (2007) Global and regional brain metabolic scaling and its functional consequences. *BMC Biol.* **5**: 18.

Karbowski J (2009) Thermodynamic constraints on neural dimensions, firing rates, brain temperature and size. *J. Comput. Neurosci.* **27**: 415-436.

Karbowski J (2011) Scaling of brain metabolism and blood flow in relation to capillary and neural scaling. *PLoS ONE* **6**: e26709.

Karbowski J (2012) Approximate invariance of metabolic energy per synapse during development in mammalian brains. *PLoS ONE* **7**: e33425.

Karbowski J (2014) Constancy and trade-offs in the neuroanatomical and metabolic design of the cerebral cortex. *Front. Neural Circuits* **8**: 9.

Karbowski J (2015) Cortical composition hierarchy driven by spine proportion economical maximization or wire volume minimization. *PloS Comput. Biol.* **11**: e1004532.

Kasai H, Matsuzaki M, Noguchi J, Yasumatsu N, Nakahara H (2003) Structure-stability-function relationships of dendritic spines. *Trends Neurosci.* **26**: 360-368.

Khakh BS, North RA (2012) Neuromodulation by extracellular ATP and P2X receptors in the CNS. *Neuron* **76**: 51-69.

Kim B, Hawes SL, Gillani F, Wallace LJ, Blackwell KT (2013) Signaling pathways involved in striatal synaptic plasticity are sensitive to temporal pattern and exhibit spatial specificity. *PloS Comput. Biol.* **9**: e1002953.

Kirkpatrick J, Pascanu R, Rabinowitz N, Veness J, Desjardins G, Rusu AA, et al (2017) Overcoming catastrophic forgetting in neural networks. *Proc. Natl. Acad. Sci. USA* **114**: 3521-3526.

Krebs EG (1981) Phosphorylation and dephosphorylation of glycogen phosphorylase: a prototype for reversible covalent enzyme modification. *Curr. Top. Cell. Regul.* **18**: 401-419.

Laughlin SB, de Ruyter van Steveninck RR, Anderson JC (1998) The metabolic cost of neural information. *Nature Neurosci.* **1**: 36-40.

Lebowitz JL, Spohn H (1999) A Gallavotti-Cohen-type symmetry in the large deviation functional for stochastic dynamics. *J. Stat. Phys.* **95**: 333-365.

Leibold C, Kempfer R (2008) Sparseness constrains the prolongation of memory lifetime via synaptic metaplasticity. *Cereb. Cortex* **18**: 67-77.

Levy WB, Baxter RA (1996) Energy efficient neural codes. *Neural Comput.* **8**: 531-543.

Li J, Wilkinson B, Clementel VA, Hou J, O'Dell TJ, Coba MP (2016) Long-term potentiation modulates synaptic phosphorylation networks and reshapes the structure of the postsynaptic interactome. *Sci. Signal.* **9**: rs8.

Lin JW, Ju W, Foster K, Lee SH, Ahmadian G, Wyszynski M, Wang YT, Sheng M (2000) Distinct molecular mechanisms and divergent endocytotic pathways of AMPA receptor internalization. *Nat. Neurosci.* **3**: 1282-1290.

Lisman J, Yasuda R, Raghavachari S (2012) Mechanisms of CaMKII action in long-term potentiation. *Nat. Rev. Neurosci.* **13**: 169-182.

Logothetis NK (2008) What we can do and what we cannot do with fMRI. *Nature* **453**: 869-878.

Matsuzaki M, Ellis-Davies GCR, Nemoto T, Miyashita Y, Iino M, Kasai H (2001) Dendritic spine geometry is critical for AMPA receptor expression in hippocampal CA1 pyramidal neurons. *Nat. Neurosci.* **4**: 1086-1092.

Mehta P, Schwab DJ (2012) Energetic costs of cellular computation. *Proc. Natl. Acad. Sci. USA* **109**: 17978-17982.

Meyer D, Bonhoeffer T, Scheuss V (2014) Balance and stability of synaptic structures during synaptic plasticity. *Neuron* **82**: 430-443.

Michalski PJ (2013) The delicate bistability of CaMKII. *Biophys. J.* **105**: 794-806.

Miller P, Zhabotinsky AM, Lisman JE, Wang X-J (2005) The stability of a stochastic CaMKII switch: Dependence on the number of enzyme molecules and protein turnover. *PLoS Biol.* **3**: e107.

Molden RC, Goya J, Khan Z, Garcia BA (2014) Stable isotope labeling of phosphoproteins for large-scale phosphorylation rate determination. *Molecular & Cellular Proteomics* **13**: 1106-1118.

Montgomery JM, Madison DV (2004) Discrete synaptic states define a major mechanism of synapse plasticity. *Trends Neurosci.* **27**: 744-750.

Nicolis G, Prigogine I (1977) *Self-Organization in Nonequilibrium Systems*. Wiley: New York, NY.

Nimchinsky EA, Yasuda R, Oertner TG, Svoboda K (2004) The number of glutamate receptors opened by synaptic stimulation in single hippocampal spines. *J. Neurosci.* **24**: 2054-2064.

O'Connor DH, Wittenberg GM, Wang SSH (2005) Graded bidirectional synaptic plasticity is composed of switch-like unitary events. *Proc. Natl. Acad. Sci. USA* **102**: 9679-9684.

Pankratov Y, Lalo U, Krishtal OA, Verkhratsky A (2009) P2X receptors and synaptic plasticity. *Neuroscience* **158**: 137-148.

Petersen CC, Malenka RC, Nicoll RA, Hopfield JJ (1998) All-or-none potentiation at CA3-CA1 synapses. *Proc. Natl. Acad. Sci. USA* **95**: 4732-4737.

Phillips R, Kondev J, Theriot J, Garcia H (2012) *Physical Biology of the Cell*. Garland Science: London.

Poo M-m, Pignatelli M, Ryan TJ, Tonegawa S, Bonhoeffer T, Martin KC, Rudenko A, Tsai L-H, Tsien RW, Fishell G, et al (2016) What is memory? The present state of the engram. *BMC Biol.* **14**: 40.

Pougnet JT, Toulme E, Martinez A, Choquet D, Hosy E, Boue-Grabot E (2014) ATP P2X receptors downregulate AMPA receptor trafficking and postsynaptic efficacy in hippocampal neurons. *Neuron* **83**: 417-430.

Qian H (2007) Phosphorylation energy hypothesis: Open chemical systems and their biological function. *Annu. Rev. Phys. Chem.* **58**: 113-142.

Qian H (2006) Open-system nonequilibrium steady state: Statistical thermodynamics, fluctuations, and chemical oscillations. *J. Phys. Chem. B* **110**: 15063-15074.

Raichle ME, Mintun MA (2006) Brain work and brain imaging. *Annu. Rev. Neurosci.* **29**: 449-476.

Rolfe DFS, Brown GC (1997) Cellular energy utilization and molecular origin of standard metabolic rate in mammals. *Physiol. Revs.* **77**: 731-758.

Sabatini BL, Oertner TG, Svoboda K (2002) The life cycle of Ca^{2+} ions in dendritic spines. *Neuron* **33**: 439-452.

Schnakenberg J (1976) Network theory of microscopic and macroscopic behavior of master equation systems. *Reviews of Modern Physics* **48**: 571-585.

Sheng M, Hoogenraad CC (2007) The postsynaptic architecture of excitatory synapses:

A more quantitative view. *Annu. Rev. Biochem.* **76**: 823-847.

Sheng M, Kim E (2011) The postsynaptic organization of synapses. *Cold Spring Harb Perspect Biol* **3**: a005678.

Shoenbaum G, Chiba AA, Gallagher M (1999) Neural encoding in orbitofrontal cortex and basolateral amygdala during olfactory discrimination learning. *J. Neurosci.* **19**: 1876-1884.

Shulman RG, Rothman DL (1998) Interpreting functional imaging studies in terms of neurotransmitter cycling. *Proc. Natl. Acad. Sci. USA* **95**: 11993-11998.

Shulman RG, Rothman DL, Hyder F (1999) Stimulated changes in localized cerebral energy consumption under anesthesia. *Proc. Natl. Acad. Sci. USA* **96**: 3245-3250.

Shulman RG, Rothman DL, Behar KL, Hyder F (2004) Energetic basis of brain activity: implications for neuroimaging. *Trends Neurosci.* **27**: 489-495.

Smith MA, Riby LM, van Eekelen JAM, Foster JK (2011) Glucose enhancement of human memory: A comprehensive research review of the glucose memory facilitation effect. *Neurosci. Biobehavior. Revs.* **35**: 770-783.

Smolen P, Baxter DA, Byrne JH (2012) Molecular constraints on synaptic tagging and maintenance of long-term potentiation: a predictive model. *PLoS Comput. Biol.* **8**: e1002620.

Sonnay S, Duarte JM, Just N, Gruetter R (2016) Compartmentalised energy metabolism supporting glutamatergic neurotransmission in response to increased activity in the rat cerebral cortex: A ¹³C MRS study in vivo at 14.1 T. *J. Cereb. Blood Flow Metab.* **36**: 928.

Sonnay S, Poirot J, Just N, Clerc AC, Gruetter R, Rainer G, Duarte JMN (2018) Astro-

cytic and neuronal oxidative metabolism are coupled to the rate of glutamate-glutamine cycle in the tree shrew visual cortex. *Glia* **66**: 477-491.

Star EN, Kwiatkowski DJ, Murthy VN (2002) Rapid turnover of actin in dendritic spines and its regulation by activity. *Nature Neurosci.* **5**: 239-246.

Sun L, Zhang Y, Hwang G, Jiang J, Kim D, et al (2018) Synaptic computation enabled by Joule heating of single-layered semiconductors for sound localization. *Nano Lett.* **18**: 3229-3234.

Takeuchi T, Duszkiewicz AJ, Morris RGM (2014) The synaptic plasticity and memory hypothesis: encoding, storage and persistence. *Phil. Trans. R. Soc. B* **369**: 20130288.

Trinidad JC, Specht CG, Thaalhammer A, Schoepfer R, Burlingame AL (2006) Comprehensive identification of phosphorylation sites in postsynaptic density preparations. *Molecular & Cellular Proteomics* **5**: 914-922.

Trinidad JC, Barkan DT, Gullede BF, Thaalhammer A, Sali A, Schoepfer R, Burlingame AL (2012) Global identification and characterization of both O-GlcNAcylation and phosphorylation at murine synapse. *Molecular & Cellular Proteomics* **11**: 215-229.

Van den Broeck C, Esposito M (2015) Ensemble and trajectory thermodynamics: A brief introduction. *Physica A* **418**: 6-16.

Visscher K, Schnitzer MJ, Block SM (1999) Single kinesin molecules studied with a molecular force clamp. *Nature* **400**: 184-189.

Volgushev M, et al (2004) Probability of transmitter release at neocortical synapses at different temperatures. *J. Neurophysiol.* **92**: 212-220.

Yoshimura Y, Yamauchi Y, Shinkawa T, Taoka M, et al (2004) Molecular constituents of the postsynaptic density fraction revealed by proteomic analysis using multidimen-

sional liquid chromatography-tandem mass spectrometry. *J. Neurochem.* **88**: 759-768.

Zhang J, Petit CM, King DS, Lee AL (2011) Phosphorylation of a PDZ domain extension modulates binding affinity and interdomain interactions in postsynaptic density-95 (PSD-95) protein, a membrane-associated guanylate kinase (MAGUK). *J. Biol. Chem.* **286**: 41776-41785.

Zhu J, Shang Y, Zhang M (2016) Mechanistic basis of MAGUK-organized complexes in synaptic development and signalling. *Nat. Rev. Neurosci.* **17**: 209-223.

Zhu F, Cizeron M, Qiu Z, Benavides-Piccione R, Kopanitsa MV, Skene NG, Koniaris B, DeFelipe J, Fransen E, Komiyama NH, Grant SGN (2018) Architecture of the mouse brain synaptome. *Neuron* **99**: 781-799.

Figure Captions

Fig. 1

Cascade model of synaptic plasticity with cyclic and noncyclic reactions.

(A) An example of the 3 state model with noncyclic reactions. For this model with a “ladder” structure EPR at steady state is zero (see the Methods), and hence this configuration is at thermal equilibrium with the environment and has a vanishing metabolic rate. This is not a realistic situation.

(B) Synaptic plasticity model with cyclic reactions. This model yields nonzero EPR and metabolic rate at steady state due to “reverberating” loop that creates a nonzero (cyclic) probability flux (see the Methods). State with the probability p_- describes a protein in a ground state, state with the probability q_0 corresponds to the protein + substrate complex, and state with the probability p_+ is the activated state of the protein + substrate complex that can signal (activate) to other downstream molecules. To initiate some function a synapse must move from the ground state p_- to state p_+ . However, direct transitions between p_- and p_+ are rare (although possible due to thermal fluctuations), and the protein has to use an alternative pathway to reach the activated state p_+ . This involves a sequence of two transitions from p_- to q_0 (binding a protein with a substrate; relatively fast), and from q_0 to p_+ (activation of the protein + substrate complex). The latter transition is powered by ATP hydrolysis ($\text{ATP} \leftrightarrow \text{ADP} + \text{P}$), which provides a necessary energy for speeding up this transition. When local concentration of ATP increases due to calcium influx, the transition rate $q_0 \rightarrow p_+$ increases accordingly. The process $q_0 \rightarrow p_+$ can be thought as protein phosphorylation, e.g., phosphorylation of CaMKII and/or PSD-95, which are the most abundant and one

of the main signaling molecules in dendritic spines (Sheng and Kim 2011). This cyclic molecular motif is known as a phosphorylation-dephosphorylation cycle and serves as a building block for constructing more complex signaling molecular networks (Hill 1989; Qian 2007).

(C) Cascade synaptic model with many basic cyclic motifs. This is an expansion of the model in panel B, and contains two chains of “up” and “down” synaptic states corresponding to binary synaptic weight or a number of AMPA receptors expressed in the spine membrane (Petersen et al 1998; O’Connor et al 2005). Occupancy probabilities in the up and down states are respectively p_k^+, q_k^+ and p_k^-, q_k^- . The transitions $p_k^\pm \leftrightarrow p_{k+1}^\pm$ are spontaneous and correspond to the direct rare transitions $p_- \leftrightarrow p_+$ in panel B. The pathway $p_k^\pm \leftrightarrow q_k^\pm \leftrightarrow p_{k+1}^\pm$ is indirect, since it involves an intermediate state q_k^\pm (corresponding to state q_0 in panel B). The reactions $q_k^\pm \rightarrow p_{k+1}^\pm$ correspond to protein phosphorylation driven by ATP hydrolysis with transition rates a_k^\pm , while the reverse reactions $p_{k+1}^\pm \rightarrow q_k^\pm$ describe much slower dephosphorylations with transition rate $\epsilon_3 b$ that is a few orders of magnitude smaller than a_k^\pm (Qian 2006, 2007). All the transition rates a_k^\pm are proportional to the amplitude a_0 . The transitions in the direction $p_k^+ \rightarrow p_{k+1}^+$ (plus $p_1^- \rightarrow p_1^+$) of the up states are associated with LTP process, whereas the transitions in the direction $p_k^- \rightarrow p_{k+1}^-$ of the down states are related to LTD. The dynamics of downstream cycles (higher index k) both for the up and down states are scaled down by a factor e^{-kz} with a characteristic slowing down factor z , which means that the transitions within deeper states are progressively slower. When the synapse is stimulated and a plasticity process initiated, only the ATP-driven rates from q_k^\pm to p_{k+1}^\pm , denoted as a_k^\pm are time dependent. Specifically, for synapses undergoing LTP the

rates a_k^+ are time dependent, while for synapses undergoing LTD the rates a_k^- change in time. The state with the occupancy p_1^- is the ground state (depressed).

Fig. 2

Dependence of baseline synaptic plasticity energy rate EPR_0 on internal synaptic parameters. Baseline EPR_0 is almost independent on the number of basic synaptic states n (upper panel; blue diamonds for $z = 0$, red squares for $z = 0.8$, yellow circles for $z = 1.5$), but it decreases monotonically with increasing the slowing-down rate z (middle panel). Dependence of EPR_0 on the ATP-driven transition rate a_0 is more complex (bottom panel): when $z = 0$ (solid line) EPR_0 increases monotonically with a_0 up to a saturation, while for $z > 0$ (dashed line for $z = 0.8$, dashed-dotted line for $z = 1.5$) EPR_0 exhibits a bimodal shape and decays to 0 for large a_0 .

Fig. 3

Time course of memory trace SNR and associated entropy production rate EPR after synaptic stimulation. Synaptic stimulation $A_{\pm}(t)$ affects the ATP driven transitions a_k^{\pm} in the following way: $a_k^{\pm} \mapsto a_k^{\pm}(t) = a_k^{\pm}[1 + A_{\pm}(t)]$, where $A_{\pm}(t) = A_{\pm} \exp(-t/\tau)$. A) $A_+(t)$, SNR, and EPR as functions of time for different stimulus amplitudes A_+ (solid blue line for $A_+ = 50$, dashed red line for $A_+ = 10$). B) $A_+(t)$, SNR, and EPR as functions of time for different stimulus durations τ (solid blue line for $\tau = 20$ min, dashed red line for $\tau = 2$ min). Note that for both cases A) and B) the SNR decays to zero as approximately a power law $\sim t^{-\delta}$ with $\delta \approx 1.3$. This is much slower decay than EPR relaxation to its baseline, which essentially follows the stimulation $A_+(t)$. Moreover, EPR stabilizes at a nonzero value, which is a signature

of a non-equilibrium steady state with a corresponding nonzero metabolic rate. For all plots $z = 1.5$.

Fig. 4

Relative cost of maintaining a memory trace can be small for progressively slower downstream synaptic transitions. Relative energy associated with a memory trace above baseline $\Delta E/E_0$ (where $\Delta E = E - E_0$, and $E_0 = \text{EPR}_0 T_m$) as a function of amplitude A_+ and duration τ of the stimulation. Note that $\Delta E/E_0$ generally gets smaller for increasing the rate of synaptic slowing down z .

Fig. 5

Effect of synaptic stimulation magnitude on memory lifetime and its energy cost. (A) Memory lifetime T_m , its energy cost E and their ratio T_m/E as functions of stimulation amplitude A_+ . (B) The same variables as functions of stimulus duration τ . Note that in both cases the ratio T_m/E is essentially constant, which indicates that longer memories need proportionally more energy. In all panels, solid blue line correspond to $z = 0$, dashed red line to $z = 0.8$, and dotted yellow line to $z = 1.5$.

Fig. 6

Memory lifetime and its energy cost as functions of the number of synaptic states n . Memory lifetime per energy is essentially constant as a function of n . Note that the relative energy above baseline for maintaining memory trace is a tiny percentage for $z > 0$ and larger n . Blue diamonds correspond to $z = 0$, red squares to $z = 0.8$, and yellow circles to $z = 1.5$.

Fig. 7

Dependence of memory lifetime and its energy cost on the fraction of potentiated synapses f . For sufficiently large f ($f > 0.2$), memory lifetime T_m , its energy cost E , as well as T_m/E and $\Delta E/E_0$ are all essentially constant. Blue solid line corresponds to $z = 0$, red dashed line to $z = 0.8$, and yellow dotted line to $z = 1.5$.

Fig. 8

Memory lifetime and its energy cost as functions of slowing-down rate z . The ratio T_m/E increases monotonically but weakly with z , and $\Delta E/E_0$ decreases with z . Blue solid line corresponds to $f = 0.2$, red dashed line to $f = 0.5$, and yellow dotted line to $f = 0.8$.

Fig. 9

Memory lifetime and its energy cost as functions of the phosphorylation rate amplitude a_0 . Surprisingly, for sufficiently large z longer memories can require less energy (two upper panels). The ratio T_m/E exhibit a minimum for some a_0 , but increases relatively fast for larger a_0 , especially for larger z . Blue solid line corresponds to $z = 0$, red dashed line to $z = 0.8$, and yellow dotted line to $z = 1.5$.

Table 1: Energetics of the major molecular processes involved in dendritic spine plasticity for rat brain.

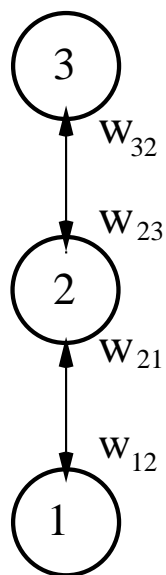
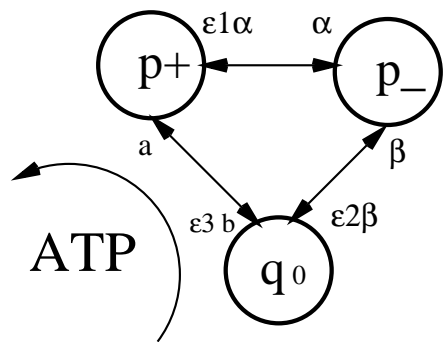
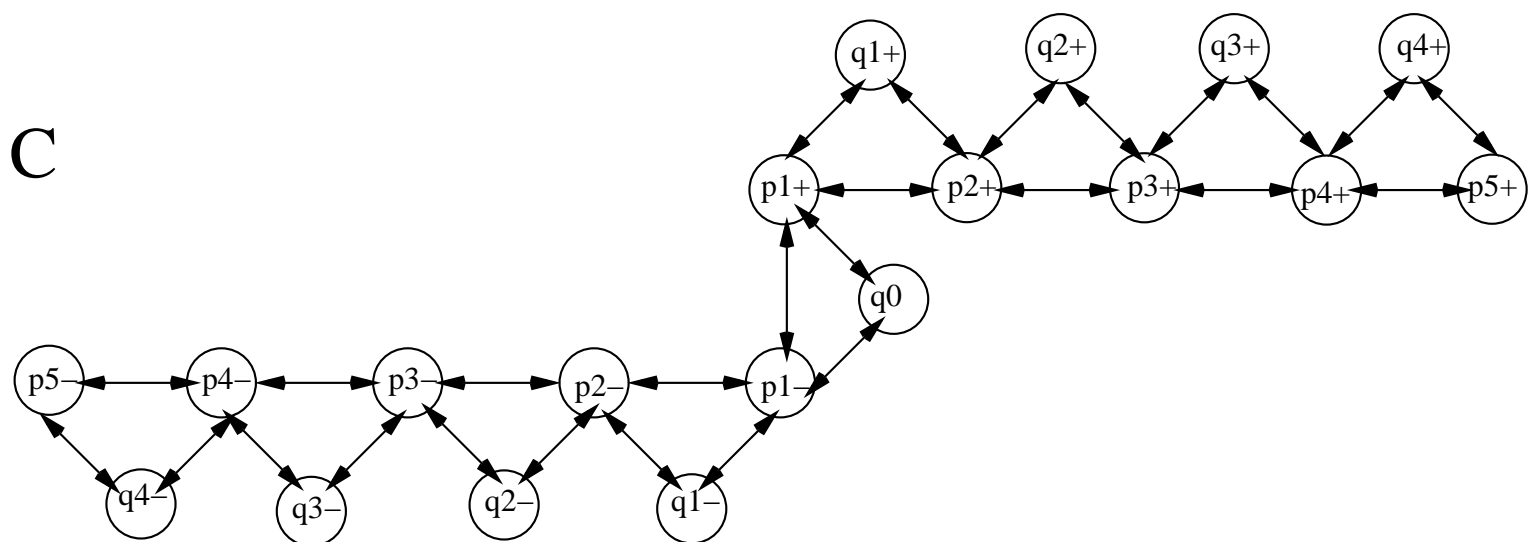
Molecular mechanism	ATP rate (min ⁻¹)
Extra-synaptic	
Glutamate recycling	1602
ATP binding to spine	60
Intra-synaptic	
Ca ²⁺ removal	6000
Protein phosphorylation: active LTP* (resting non-LTP)	310000 – 910000 (7500)
Protein synthesis	3700
Actin treadmilling	8000
Receptor trafficking: movement insertion	8184 18.7
Modulatory	
P2X receptors	2871

* Values depend on Ca²⁺ stimulation rate.

Table 2: Comparison of the metabolic costs of synaptic plasticity and fast excitatory synaptic transmission for rat brain.

Synaptic plasticity total cost (ATP/min)	Postsynaptic current cost (ATP/min)	Plasticity/Transmission relative cost (%)
$(3.4 - 9.4) \cdot 10^5$ (enhanced phosphorylation)	$8.4 \cdot 10^6$	4.0 – 11.2

The cost of the postsynaptic current (synaptic transmission) is estimated based on Attwell and Laughlin (2001).

A**B****C****Figure 1**

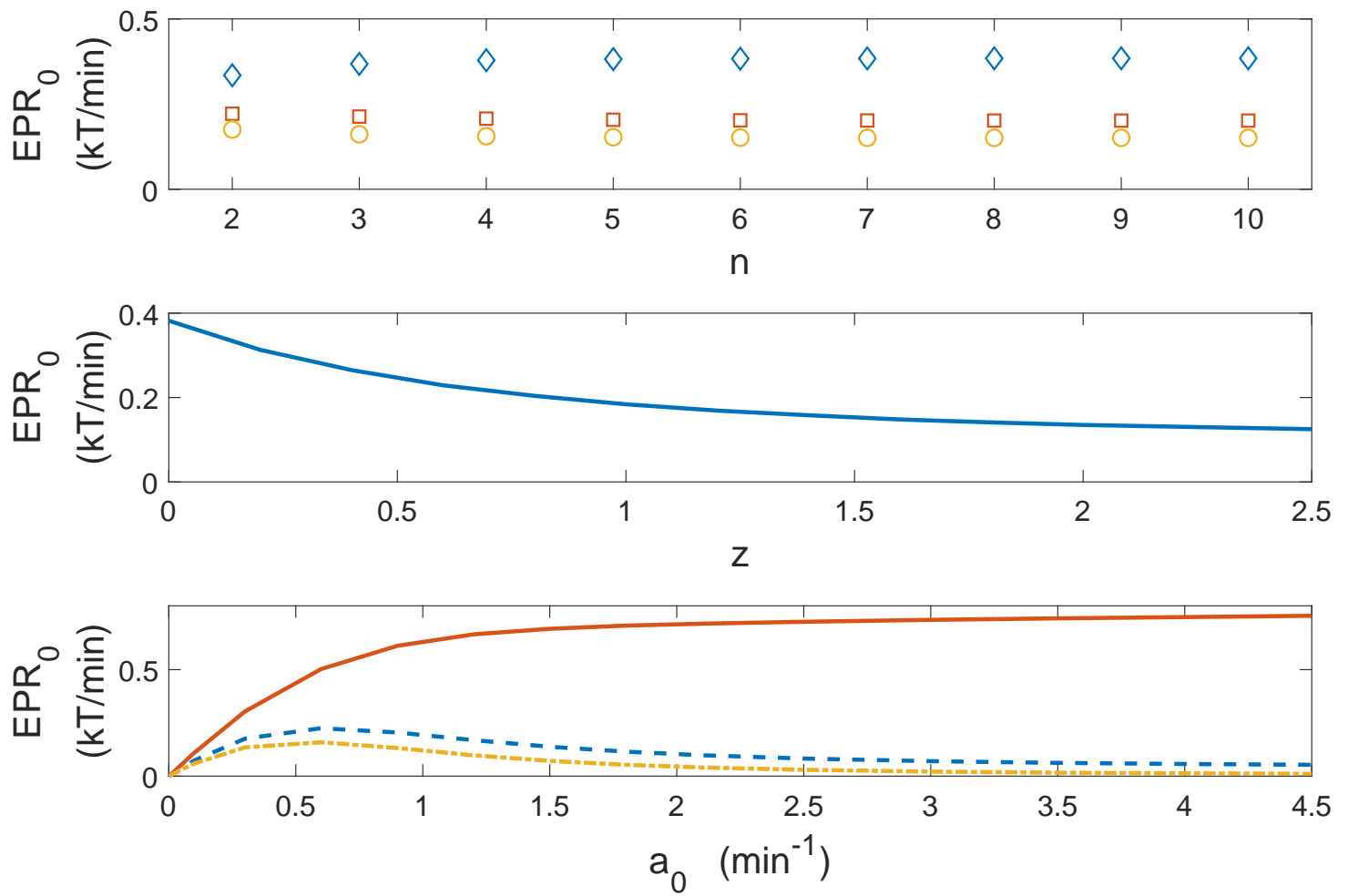


Figure 2

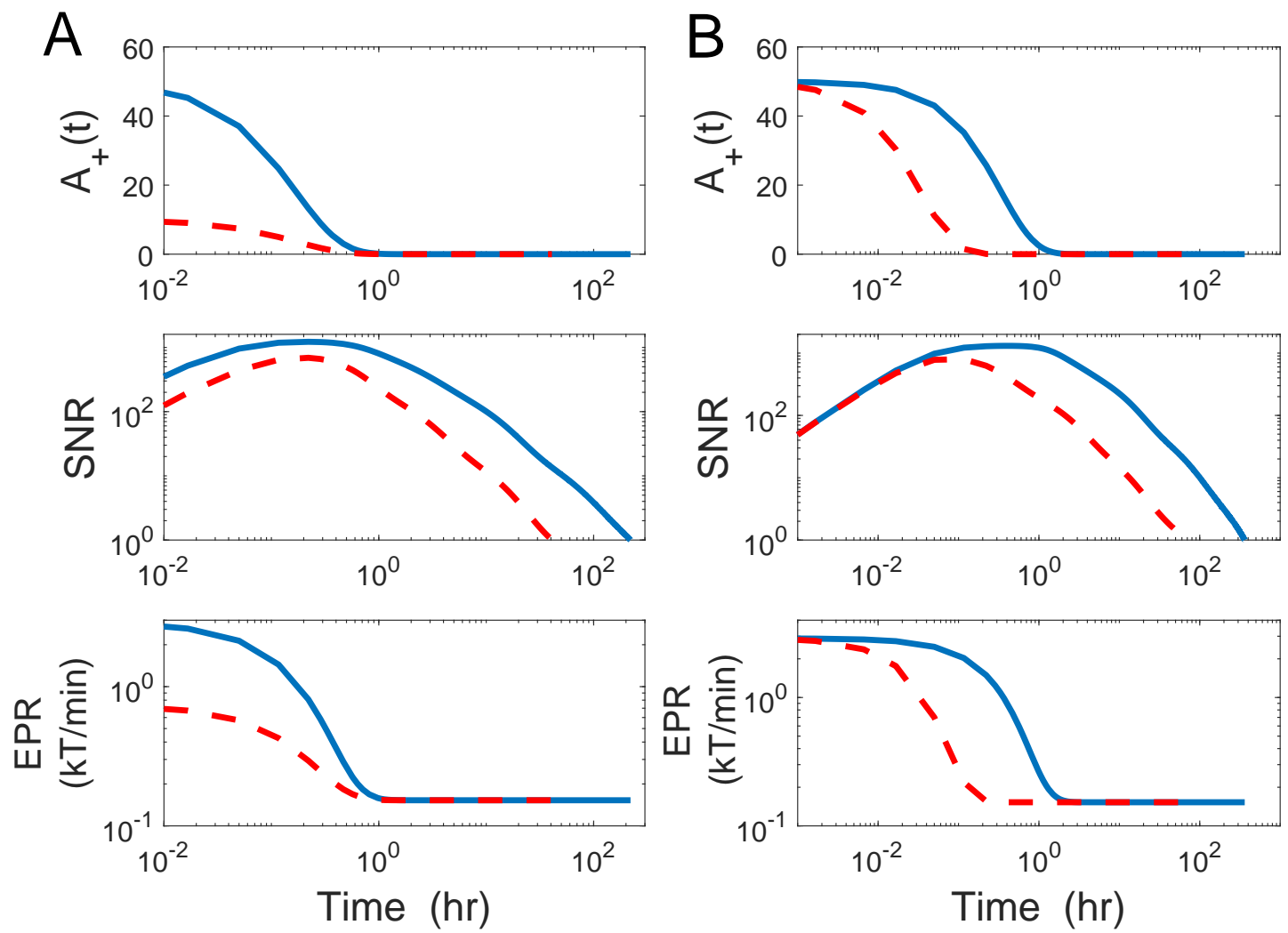


Figure 3

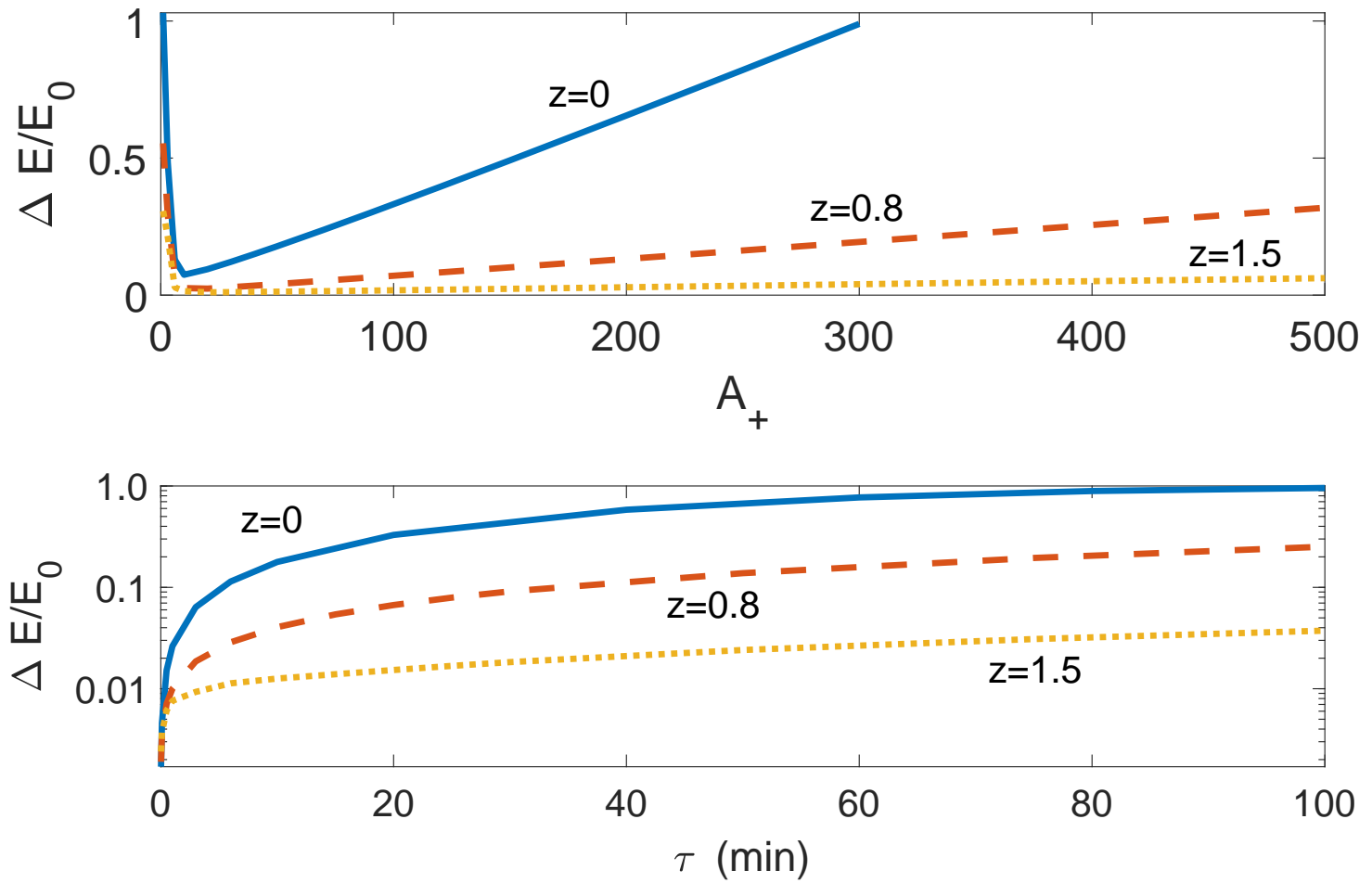


Figure 4

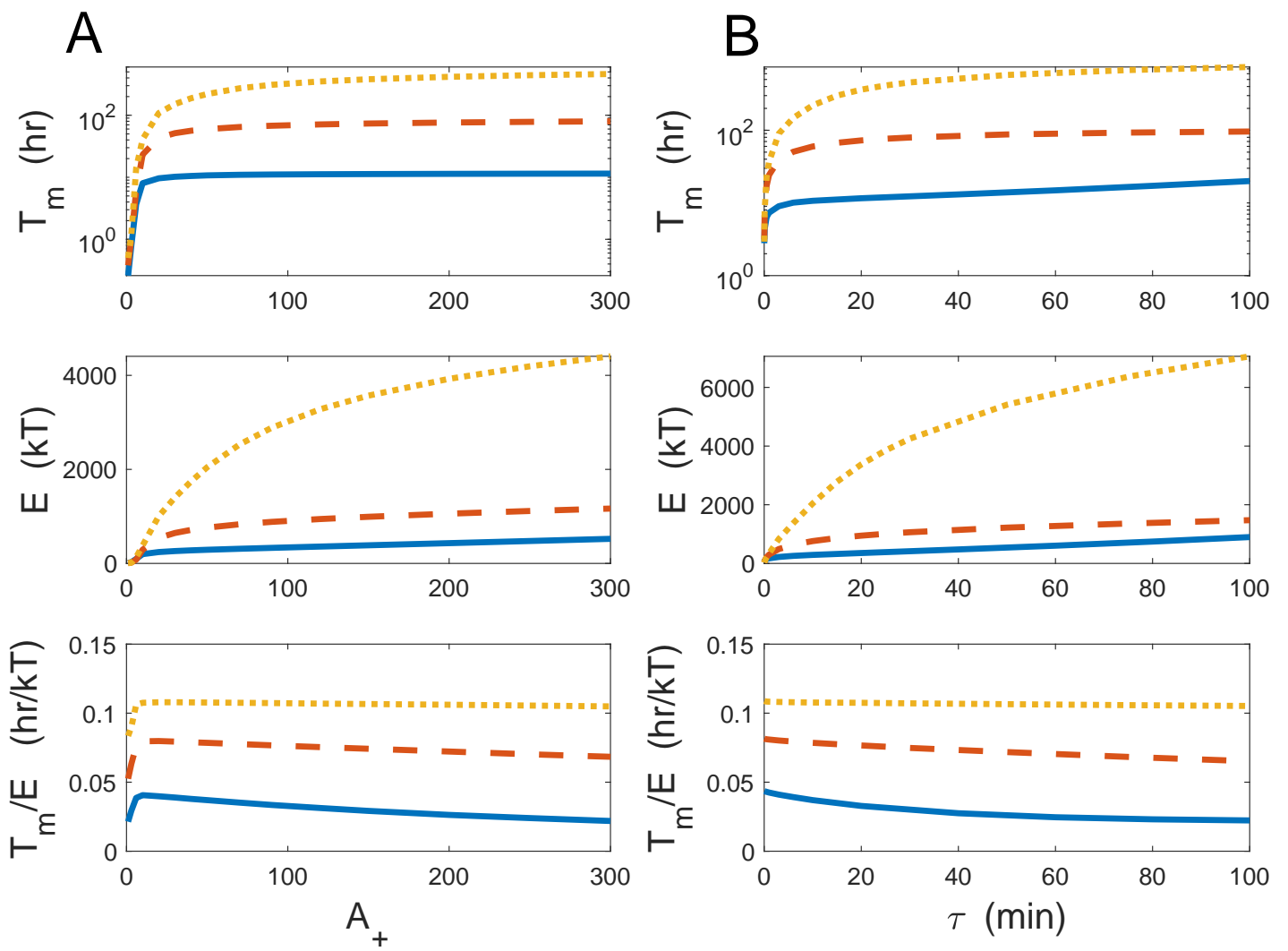


Figure 5

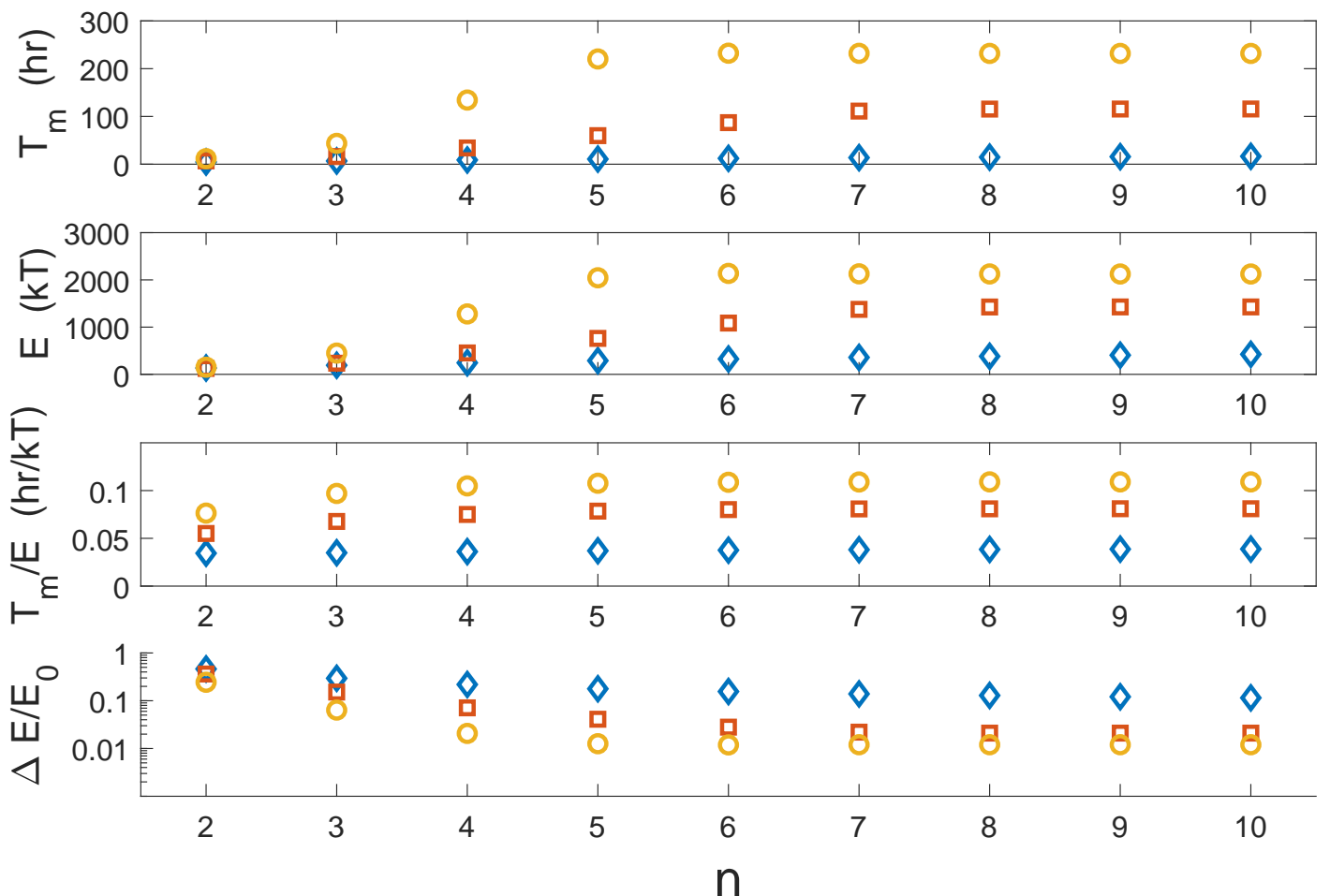


Figure 6

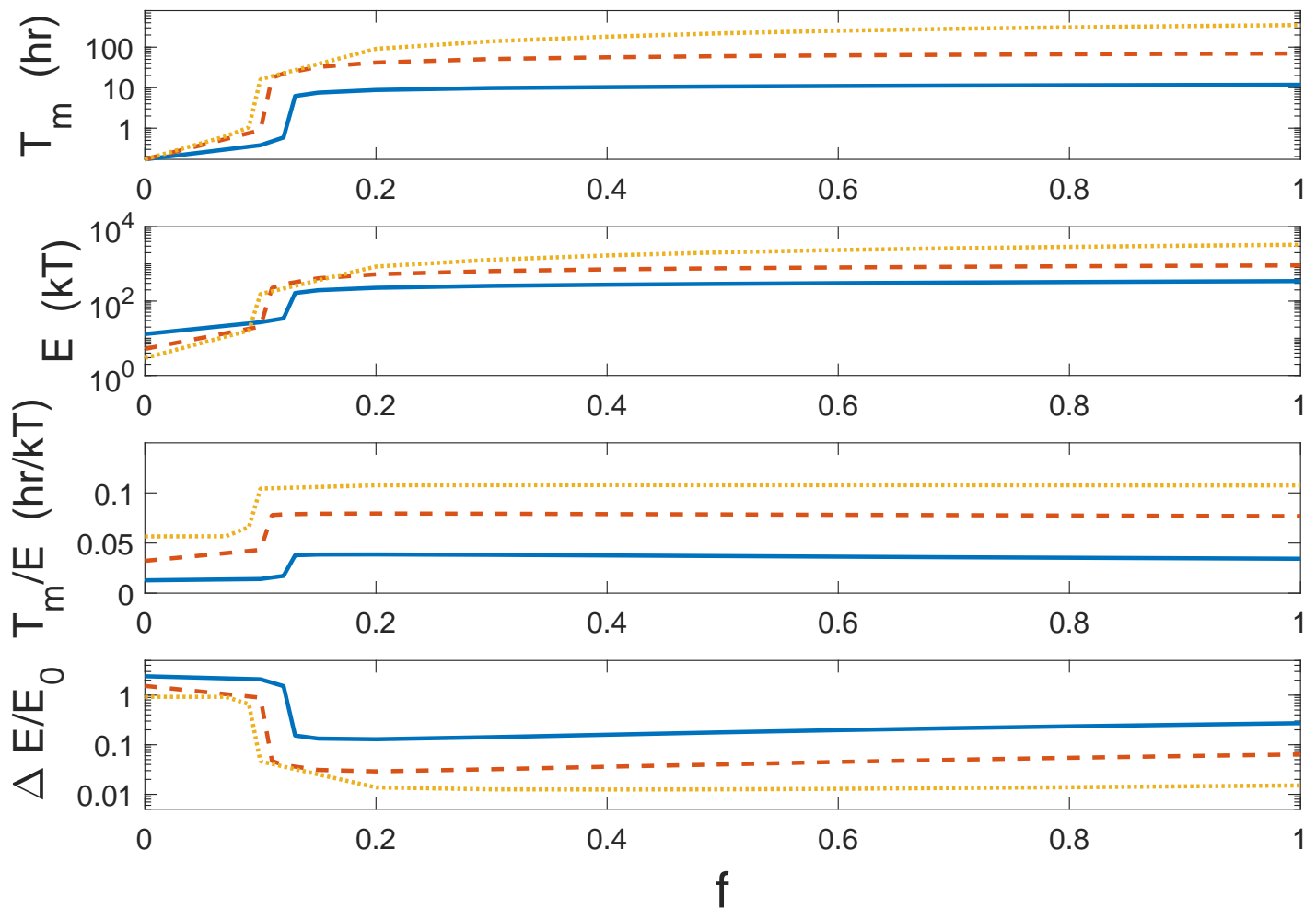


Figure 7

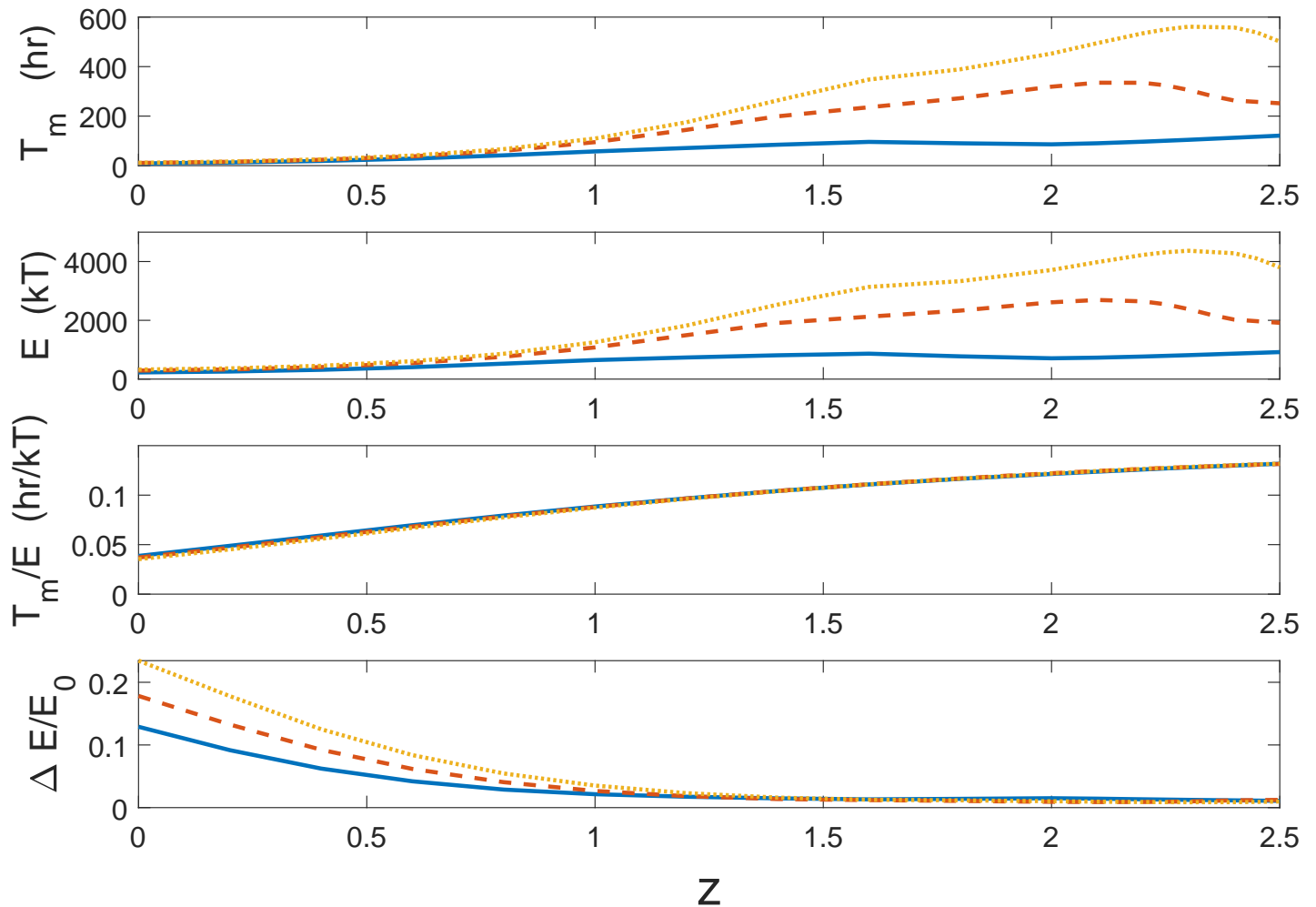


Figure 8

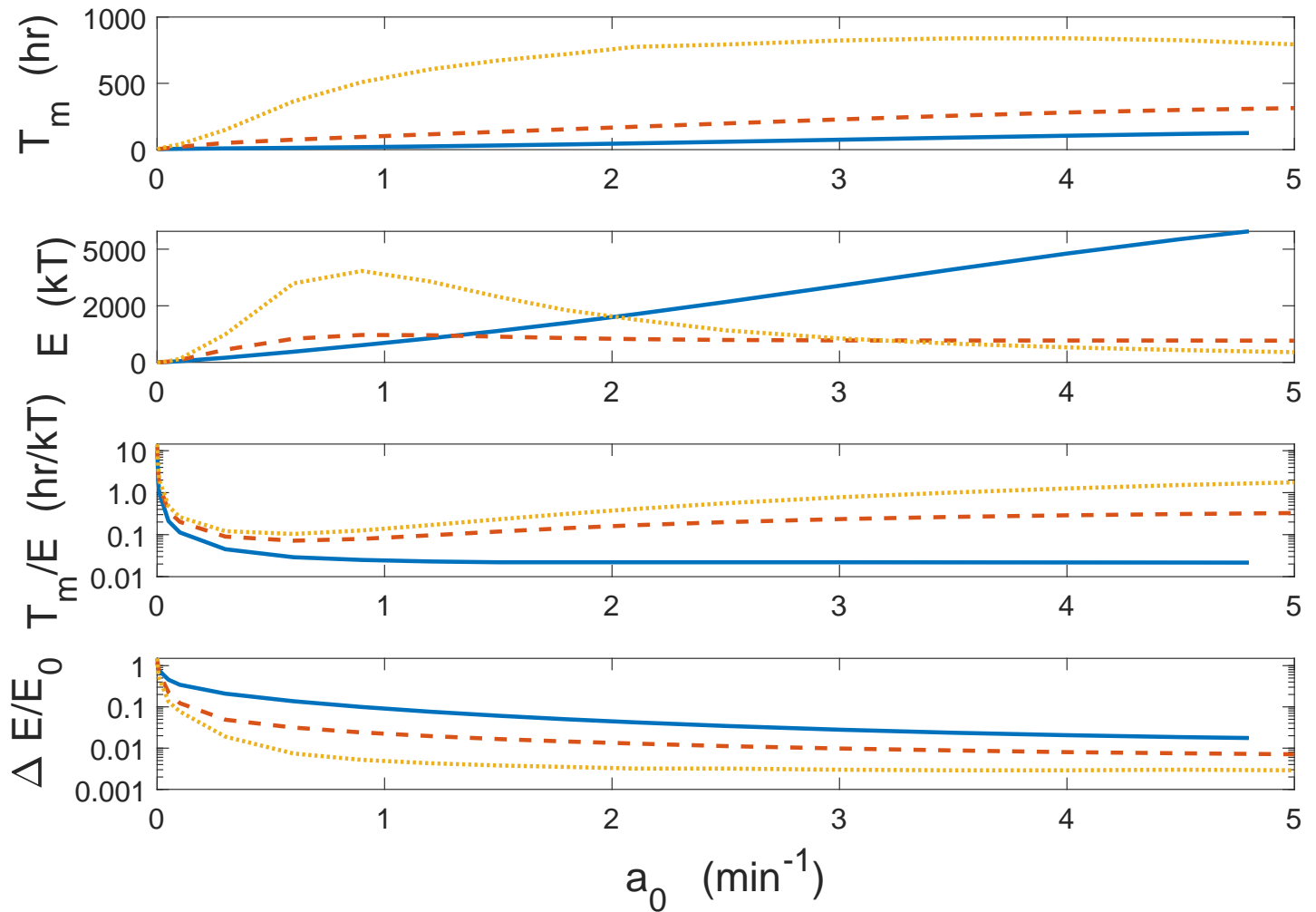


Figure 9